

**SULFUR ISOTOPE AND FLUID INCLUSION STUDY OF FLUID
SOURCES WITHIN THE FRESNILLO SOUTHWEST SILVER DISTRICT,
ZACATECAS, MEXICO**

by

Matthew A. Earthman

Submitted in Partial Fulfillment of the Requirements for the

Degree of Master of Science in Geochemistry

New Mexico Institute of Mining and Technology

Earth and Environmental Science Department

Socorro, New Mexico

June, 2010

ABSTRACT

The Fresnillo Mining District in Zacatecas, Mexico, is a large, intermediate sulfidation epithermal-style deposit consisting of high-grade silver and significant lead and zinc. Over the past six years, several extensive veins have been discovered approximately 8 kilometers southwest of the historic Proaño-Fortuna Fresnillo deposits, further enlarging this already massive silver district. To better understand the formation and genesis of the new veins, and their relation to previously known mineralization, reflected light petrography, stable isotopes, and fluid inclusion analyses were performed on 75 samples from 36 vein intercepts from 5 of the new prospect veins.

The Fresnillo Southwest veins have a similar paragenesis to what has been found in the previous studies of Fresnillo Southeast, with five main stages of mineralization. Mineralogy within the veins is dominated by quartz, calcite, adularia, sphalerite, galena, pyrite, and arsenopyrite, with most silver present within silver sulfosalts. Samples from drill hole intercepts of veins of the Fresnillo-Southwest district were analyzed for stable isotopes and fluid inclusion microthermometry. $\delta^{34}\text{S}$ values of the sulfides are relatively consistent, with average values of -4.5 ± 1.2 ‰ for pyrite (n=39), -4.8 ± 0.8 ‰ for sphalerite (n=45), and -6.9 ± 0.9 ‰ for galena (n=29). A single pyrite nodule from the sedimentary host rocks yielded a $\delta^{34}\text{S}$ value of -26 ‰. Mineral $\delta^{18}\text{O}$ values from quartz and calcite from within the Valdecañas vein range from 12.3 to 16.8 ‰ (n=9) and 7.4 to 12.9 ‰ (n=13), respectively. Fluid inclusion waters analyzed by thermal decrepitation returned δD values ranging from -79 to -54 ‰ (n=5). Homogenization temperatures

from ore-stage quartz range from 180 to 310°C (mode of 260°C), and fluid salinities from 0.5 to 11 wt. % NaCl equivalent (mode of 2.5%).

Using fluid inclusion homogenization temperatures and mineral isotope values, the composition of the ore forming fluid was calculated. The $\delta^{34}\text{S}$ of H_2S of the ore forming fluid from pyrite (-7.5 to -4.5 ‰) were slightly lighter than the $\delta^{34}\text{S}_{\text{H}_2\text{S}}$ from sphalerite (-6 to -4 ‰) and galena (-6.5 to -3.5 ‰). Calculated $\delta^{18}\text{O}$ fluid values from quartz and calcite range from 5.0 to 11.5 ‰. By incorporating the δD values from fluid inclusion waters and pairing them with $\delta^{18}\text{O}$ of waters calculated from quartz, it can be determined that the water within the Fresnillo system is either of a magmatic origin or represents highly exchanged meteoric water. These values agree with earlier studies from the Fresnillo deposits.

The consistent $\delta^{34}\text{S}$ fluid values between the studied veins and the previously studied Fortuna-Proaño deposits suggest that the deposits were formed from a common source of sulfur throughout the entire district, and thus could be related to a single ore-forming event. The $\delta^{34}\text{S}$ values at Fresnillo are significantly lighter than what is common in most epithermal systems, and are likely the result of the incorporation of light sedimentary sulfide from the sedimentary host units into an ore fluid dominated by magmatic sulfur. This process could be accomplished through two processes: 1) leaching of sulfur from deeply circulating meteoric fluids and incorporation into ore fluids, or 2) assimilation of Guerrero Terrain into the intrusion. Gas analysis data from Velador (2010) suggests meteoric fluids were a significant portion of the ore-forming fluids, but do not provide sufficient evidence to resolve this question.

Keywords: Epithermal Deposits, Stable Isotopes, Fluid Inclusions

ACKNOWLEDGEMENTS

I would like to extend my greatest thanks to Fresno PLC and the Peñoles Corporation for the financial support that allowed this study to take place. I would also like to thank the Don Yardley fellowship, and one of its contributors, the late Mike Fitzgerald, for funding my Research Assistanceship while here at New Mexico Tech. I would also like to thank my advisor Dr. Andrew Campbell for all of his input and help over the past several years. Lastly, I would like to extend my greatest appreciation to my wife, Natalie, my parents Mark and Janie, and my friends who constantly helped and supported me while working on this project.

TABLE OF CONTENTS

ABSTRACT.....	ii
ACKNOWLEDGEMENTS.....	ii
TABLE OF CONTENTS.....	iii
LIST OF FIGURES	v
LIST OF TABLES.....	vii
INTRODUCTION	1
BACKGROUND	2
Location.....	2
History and Production.....	2
District Layout.....	3
GEOLOGY	4
Geologic Units.....	4
Sedimentary Units.....	4
Igneous Units	6
Structure	6
Vein Morphology	7
METHODS	8
Petrography	8
Fluid Inclusion Microthermometry	8
Stable Isotopes.....	8
Sulfide Mineral $\delta^{34}\text{S}$	8
Carbonate $\delta^{18}\text{O}$ and $\delta^{13}\text{C}$	9
Fluid Inclusion Deuterium	10
Silicate $\delta^{18}\text{O}$ Analysis	10
RESULTS	11
Mineral and Metal Zonation.....	11
Optical Petrography.....	13
Paragenesis	14
Fluid Inclusions	17
Inclusion Types.....	18
Microthermometry	18
Stable Isotopes.....	20
Sulfur Isotopes	20

Carbon, Oxygen, and Hydrogen Isotopes	24
INTERPRETATIONS	25
Fluid Inclusions	25
Stable Isotope Geothermometry	28
Sulfide Minerals	28
Quartz and Carbonate	30
Sulfur Isotopes	30
Carbon, Oxygen, and Hydrogen Isotopes	33
FLUID SOURCE DISCUSSION	36
CONCLUSIONS.....	42
REFERENCES	44
APPENDIX I. VALDECAÑAS VEIN SAMPLE INFORMATION	48
Sample Location Longitudinal Section	48
Valdecañas Vein Sample List.....	48
APPENDIX II. PETROGRAPHIC DESCRIPTIONS BY DRILL HOLE AND SAMPLE NUMBER	52
APPENDIX III. FLUID INCLUSION DATA	58

LIST OF FIGURES

- Figure 1. Map of Mexico highlighting the state of Zacatecas. Inset in upper right shows relative locations of several different epithermal deposits within Zacatecas, including Fresnillo, Zacatecas, and Sombrete. p. 2
- Figure 2. Map of the Fresnillo mining district with the three district zones highlighted in red (Fresnillo SW), blue (Fresnillo SE), and green (Fortuna-Proaño). Red lines represent vein locations projected to the surface. p. 4
- Figure 3. Stratigraphic Column of the Guerrero Terrane within the Fresnillo Southwest district. p. 5
- Figure 4. Longitudinal section of the Valdecañas vein, looking north summarizing lead and zinc grades. p. 12
- Figure 5. Longitudinal section of the Valdecañas vein, looking north summarizing gold equivalent grades. p. 12
- Figure 6. Thin section photomicrographs. A) Large, euhedral quartz crystals with late calcite filling void space to the outside (Sample GB-02, 728m). B) Large quartz grain with intergrown adularia. (Sample WC-01, 656m) p. 13
- Figure 7. Sphalerite with exsolved chalcopyrite and acanthite. Sample (EF-04, 831m) p. 14
- Figure 8. Different mineralizing stages within the Valdecañas vein. p. 15
- Figure 9. Paragenetic sequence of minerals within the Valdecañas vein. p. 17
- Figure 10. Fluid inclusion temperatures of homogenization for the Valdecañas Vein. *Stage III* represents the main ore stage of mineralization. p. 19
- Figure 11. Calculated salinities (from melting point depression measurements) computed from the equations of Bodnar (1993). p. 20
- Figure 12. Histogram of aqueous H₂S $\delta^{34}\text{S}$ values from different minerals within the Valdecañas vein. p. 23
- Figure 13. Histogram representing distribution of $\delta^{34}\text{S}$ H₂S values from five veins in the Fresnillo Southwest district p. 24
- Figure 14. Salinity vs. homogenization temperature of measured inclusions within the Valdecañas vein. p. 26

Figure 15. Longitudinal section of Valdecañas vein showing sampled drill intercepts and homogenization temperature gradient.	p. 27
Figure 16. Longitudinal section of Valdecañas vein showing sampled drill intercepts and fluid inclusion salinities.	p. 27
Figure 17. Speciation of aqueous sulfur species at different pH and oxygen fugacities.	p. 32
Figure 18. Histograms of calculated H ₂ S values from pyrite, sphalerite, and galena from several different veins within Fresnillo Southwest.	p. 33
Figure 19. δD vs. $\delta^{18}O$ of water calculated from quartz mineral values and fluid inclusion water.	p. 34
Figure 20. $\delta^{13}C$ vs $\delta^{18}O$ plot of analyzed calcite minerals. Shaded blue box represents typical magmatic carbonate values.	p. 36
Figure 21. Mineral $\delta^{34}S$ values from epithermal systems from around the globe grouped by each author's interpretation of sulfur source.	p. 38
Figure 22. Cross sections representing two sources of the ore forming fluid and the incorporation of sulfur into the system.	p. 40

LIST OF TABLES

Table 1. Mineral $\delta^{34}\text{S}$ values from veins within Fresnillo Southwest.	p. 21
Table 2. $\delta^{18}\text{O}$, δD , and $\delta^{13}\text{C}$ values from the Valdecañas vein.	p. 25
Table 3. Stable isotope geothermometry of sphalerite-galena and quartz-calcite mineral pairs within the Valdecañas and Jarillas veins.	p. 29

INTRODUCTION

The Fresnillo Silver District, in Zacatecas, Mexico, is an immense resource of silver, lead, zinc, and minor gold. Classified as an intermediate sulfidation system (Camprubí and Albinson, 2007), this district has been continually mined since the 1500s. Recently, in 2003, several new veins were discovered to the southwest of the active portion of Fresnillo, further enlarging this already massive district. Using several geochemical techniques, including carbon, oxygen, hydrogen, and sulfur stable isotope analysis and fluid inclusion studies, the origin and formation of these new veins can be better understood.

This study hopes to address the characteristics of the fluids and processes that formed the Fresnillo Southwest district. Fluid inclusion microthermometry on gangue mineralogy within the Valdecañas and Jarillas veins within the Fresnillo Southwest area documents the temperatures and the salinity of the ore forming fluids. This information, particularly temperatures, can then be used in conjunction with stable isotope studies to gain information on the sources of the fluids and the evolution of the fluids across the area. By comparing the information of the Fresnillo Southwest area to previous studies within the Fresnillo Southeast area, the formation of the district can be further constrained and used to understand the processes occurring in these types of epithermal systems.

BACKGROUND

Location

The Fresnillo District is located in the central region of Mexico (Figure 1), immediately south of the town of Fresnillo at an elevation of 2,100 meters (6800 feet) above sea level. Fresnillo is a city of approximately 110,000 people, and is 70 kilometers north of the city of Zacatecas. Fresnillo is located within a broad valley, flanked by the Valdecañas mountain range to the west.



Figure 1. Map of Mexico highlighting the state of Zacatecas. Insert in upper right shows relative locations of several different epithermal deposits within Zacatecas, including Fresnillo, Zacatecas, and Sombrete.

History and Production

Mining at Fresnillo began in the late 1500s shortly after the town was founded by Francisco de Ibarra in 1554. Since its establishment, the mine has been worked almost

continuously, making it one of the oldest, continuously mined deposits in North America. Up until the 1940s, most of the mining was small-scale and was limited to mining of silver oxides in near-surface operations (Gemmell et al., 1988). In the 1950s, waning reserves inspired the mine to increase brownfield exploration, and in 1976, the Santo Niño vein was discovered. This vein is the subject of most previous geologic and geochemical studies at the mine.

As of 1988, the Fresnillo district had produced over 10,000 metric tons of silver, and half a million tons each of zinc and lead (Ruvalcaba-Ruiz and Thompson, 1988). Since 1988, production has increased significantly, and since 2005, the mine has maintained annual productions of over 33 million ounces of silver, 20 thousand ounces of gold, and 38 thousand tons of lead and zinc combined (Fresnillo PLC, 2010). This astonishing rate of production makes Fresnillo one of the largest silver producers in the world (National Mining Association, 2008). With the discovery of the Southwest Fresnillo veins, this production will only increase.

District Layout

Fresnillo can be divided into several zones: the Fortuna-Proaño area, the Fresnillo Southeast area, and the Fresnillo Southwest area. The historical district, Fortuna-Proaño, is located near the base of Cerro Proaño, and consists of upwards of 150 veins that have been mined over the past 4 centuries (Ruvalcaba-Ruiz and Thompson, 1988). The Fresnillo SE section is the currently productive zone of the district, and includes the Santo Niño, San Carlos, Santa Elena, San Mateo, and San Ricardo veins, and is located about one kilometer southeast of the historical district (Figure 2). The recently discovered veins of Fresnillo Southwest, including the Valdecañas, Santa Natalia,

Saucito, and Jarillas veins, are located approximately 8 kilometers to the southwest of the Santo Niño vein.

The focus of this study includes the Valdecañas vein of the Fresnillo Southwest area, but sulfur isotope data was also collected for several other Fresnillo Southwest veins.

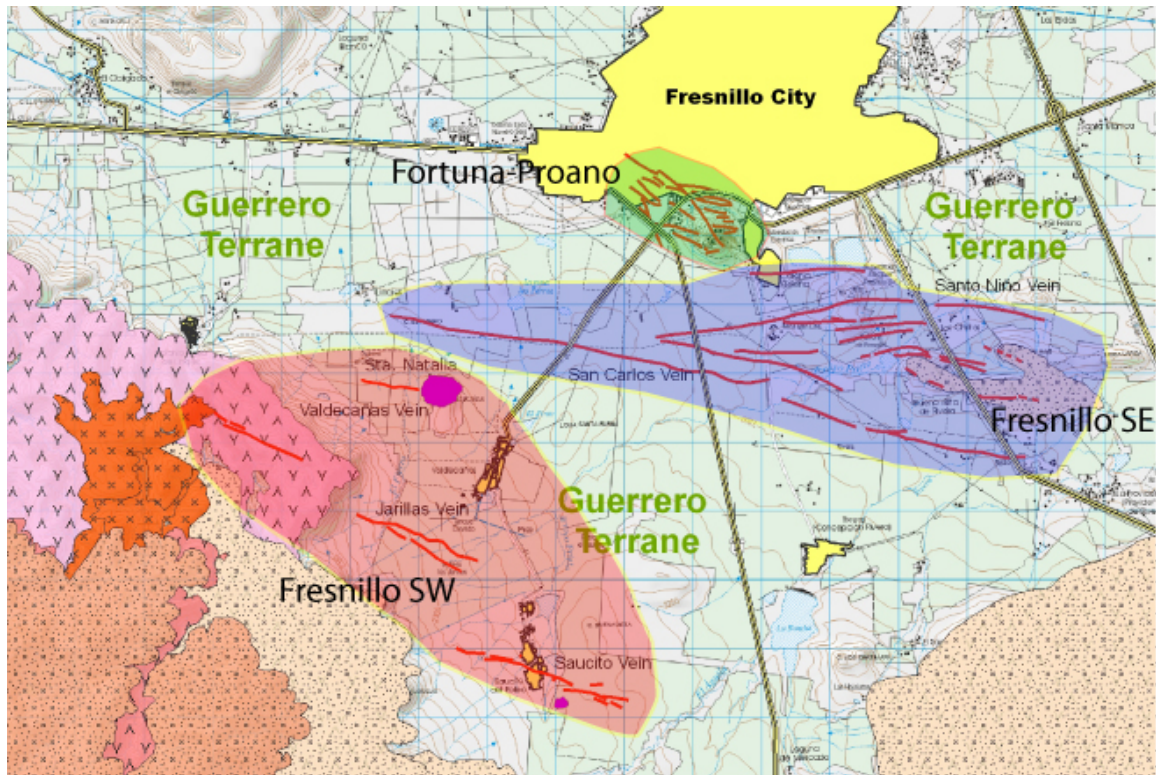


Figure 2. Map of the Fresnillo mining district with the three district zones highlighted in red (Fresnillo SW), blue (Fresnillo SE), and green (Fortuna-Proano). Red lines represent vein locations projected to the surface.

GEOLOGY

Geologic Units

Sedimentary Units

Guerrero Terrane The Fresnillo Southeast and Fresnillo Southwest veins are located almost exclusively within Cretaceous marine sediments. Traditionally, these

sediments, consisting of greywackes, shales, and thin limestones, were broken into several formations, including the upper and lower graywackes of the Proaño Group. This formation scheme was utilized in the publications of (Benton, 1991; De Cserna, 1976; Dilley, 1993; Gemmell et al., 1988; Lang et al., 1988; Ruvalcaba-Ruiz and Thompson, 1988). Recently, however, the marine sediments and volcanics have been incorporated into the Guerrero Terrane, a much larger assemblage that spans much of western and central Mexico; this assemblage is informally divided into black shales, gray sandstones (including greywackes), and andesitic and mafic volcanics (Figure 3).

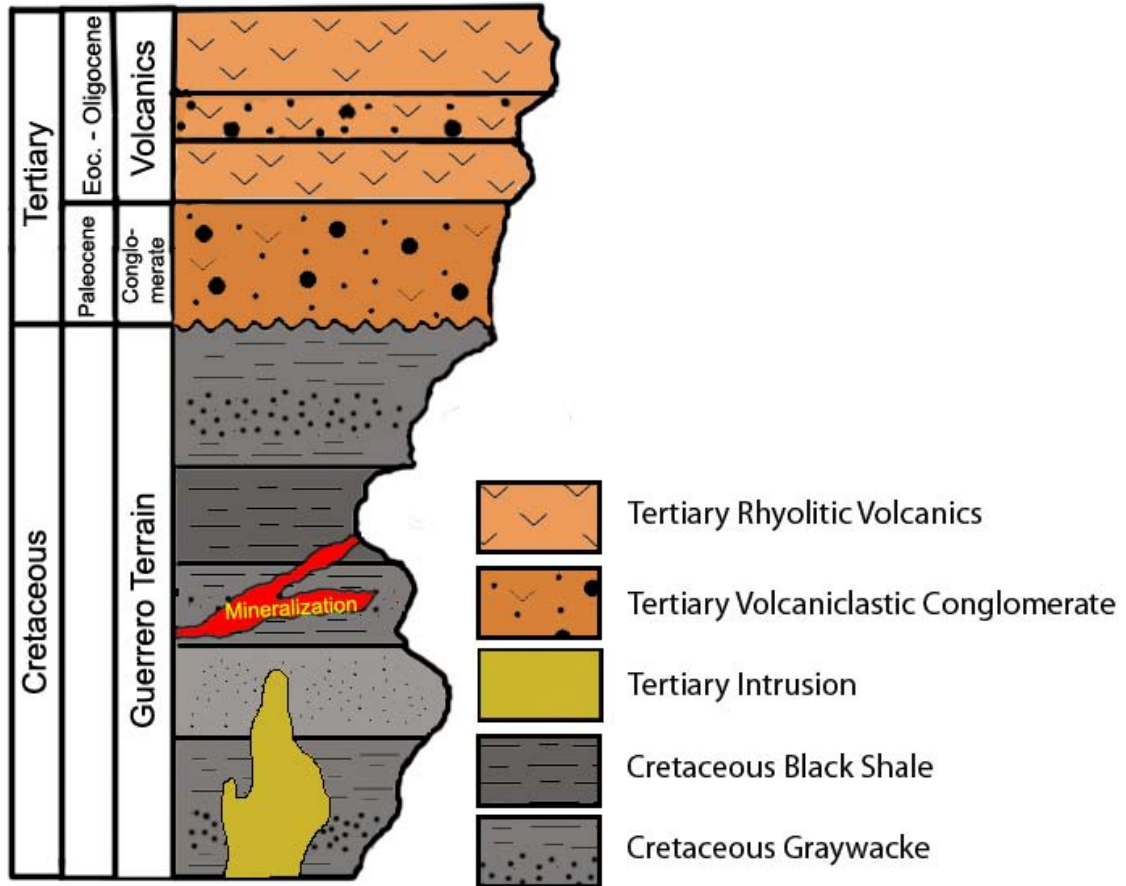


Figure 3. Stratigraphic Column of the Guerrero Terrane within the Fresnillo Southwest district.

Igneous Units

Tertiary Volcanic Units. Eocene and Oligocene rhyolites and late Miocene-Pliocene basalts (Lang et al., 1988; Velador, 2010) are present in some portions of the Fresnillo district. The rhyolites are dominantly tuffs with some sanidine and quartz phenocrysts, and have thicknesses up to 400 meters (De Cserna, 1976). The rhyolites form a large portion of the Valdecañas range, and directly overlie Guerrero Terrane in the western portions of the Fresnillo Southwest district.

Igneous Intrusions. Several intrusions cut the bedded units of the Fresnillo district. The Fortuna shaft, one of the deepest shafts within the Cerro Proaño area, intersects the Fortuna Stock, a large, cylindrical quartz monzonite. Andesitic dikes are also present in lower mine levels within this area, and they cut rocks within the Valdecañas Formation. In addition to the andesites, rhyolitic dikes are scattered throughout the district. According to K-Ar dating performed by Lang et al. (1988), these intrusions range in age from 38-30 Ma (Oligocene). Recent Ar/Ar geochronology studies by (Velador, 2010) provide much higher precision, with an age of 32.65 ± 0.05 Ma for the Fortuna Stock.

Structure

The Fresnillo district has been influenced by two different deformational events: a compressional regime in the middle to late Cretaceous, and an extensional, block faulting event in the middle to late Tertiary characterized by a period of thrust faulting and folding. The compressional events resulted in the formation of a broad, southeast-plunging anticlinorium near Cerro Proaño. This deformational event caused moderate

deformation and “crumpling” of Proaño (Guerrero) Group sediments (Gemmell et al., 1988).

The block-faulting event of the Tertiary is responsible for the Fresnillo fault, a major normal fault trending southeast. This fault down-dropped Tertiary sediments to the north adjacent to Cretaceous units to the south, and has a displacement of about 300 meters (De Cserna, 1976). Importantly, much of mineralization around Cerro Proaño are in the immediate vicinity of the fault.

Vein Morphology

The Southwest Fresnillo vein deposits are located within a radius of 4 kilometers from each other, and trend roughly NW-SE (Figure 2).

Current models based on exploration drilling suggest the Valdecañas vein has a strike length of 2 kilometers, and a vertical extent of 500 meters. The average width of the vein is approximately 5 meters, with vein intercepts averaging 500 g/ton silver and 2 g/ton gold.

The mineralization within the Valdecañas vein exhibits a variety of textures and banding. Earlier stages typically are hydrothermal breccias cemented by quartz or sulfide minerals. Later stages exhibit thin, crustiform banding and laminations of quartz, calcite, and sulfide minerals. The veins have a sigmoidal morphology (Petersen, 1990), with highly sinuous ore bands.

METHODS

Petrography

Reflected and transmitted light petrography was conducted on 20 polished thin sections from 10 vein intercepts within the Valdecañas vein. All observations were conducted on an Olympus BH-2 petrographic microscope with reflected and transmitted light capability.

Fluid Inclusion Microthermometry

Fluid inclusion studies were performed on 20 doubly-polished thick sections from 9 drill core intercepts within the Valdecañas vein system. Sixteen sections were prepared from *Stage III* (main ore stage) of mineralization, with the remaining four from *Stage V*. All measurements were completed on a Leitz SF-43 Petrographic microscope with a Linkam THMS-600 microthermometry stage, equipped with a Linkam PR-600 microthermometry controller and a CS-196 cooling system. Measurements were calibrated using the melting points of CO₂, pure water, and potassium chromate. Homogenization temperatures are accurate to ± 2 °C, and melting point temperatures were measured with a precision of ± 0.1 °C.

Stable Isotopes

Sulfide Mineral $\delta^{34}\text{S}$

Mineral separates for sulfur isotope analysis were acquired by drilling thin section billets or by hand picking. The drilling technique proved to be very effective, and allowed for 95% purity of the majority of mineral separates. Sphalerite, which can contain

upwards of 10% disseminated pyrite or exsolved chalcopyrite and silver sulfides, is the only mineral separate with the potential of significant contamination. Hand picking samples was not as precise, but close examination of samples under a binocular microscope allowed for consistent and clean mineral separates.

All sulfur isotope analyses were performed using the Delta XP IRMS in conjunction with a Costech EA 4010 Elemental Analyzer and a Conflo II gas delivery system. Powdered samples were combusted within small tin vessels at a temperature of 1020°C with oxygen to produce SO₂ gas, passed through a gas chromatograph, and then released into the mass spectrometer. Using laboratory standard gas as a reference, as well as international mineral standards (NBS-128, NZ2), the samples were analyzed for δ³⁴S and expressed relative to CDT. Twenty-eight sample duplicates were analyzed over the course of data collection; by taking the difference between these duplicates and dividing by two, an analytical precision of ± 0.2 ‰ can be attributed to this type of analysis.

Carbonate δ¹⁸O and δ¹³C

Carbonate samples from within the veins were analyzed for both δ¹³C and δ¹⁸O isotope values. Samples were either handpicked or drilled from billets, and then powdered.

All samples were run on a Finnigan Delta XP Plus Isotope Ratio Mass Spectrometer in conjunction with a PAL autosampler and Gas Bench II continuous flow gas delivery system. 0.25mg of powdered calcite was measured into glass vials, flushed with He, and treated with 100% phosphoric acid. After equilibrating for 4 hours, the resulting CO₂ gas was analyzed for δ¹³C and δ¹⁸O. Mineral standards (NBS-18, Solenhofen Limestone, and IAEA CO-9) within the run allowed for correction of the data

to PDB ($\delta^{13}\text{C}$) and VSMOW ($\delta^{18}\text{O}$) standards. Two duplicate samples within runs indicate an analytical precision of ± 0.1 ‰.

Fluid Inclusion Deuterium

Inclusion fluids for deuterium isotope analyses were extracted using thermal decrepitation. Quartz samples with a mass of 20-50mg were loaded into small silver cups, and placed into an autosampler on a Thermo-Finnigan TC/EA. The samples dropped directly in the TC/EA reactor running at 1450°C. The heat decrepitates fluid inclusions within the samples, and liberates water vapor. The vapor reacts with reduced carbon in the reactor, and forms H_2 gas. This gas was then analyzed on the mass spectrometer against a reference gas. Two mineral standards, HEKA benzoic acid and IAEA-CH7, were also run with the samples to produce a calibration curve to express the values relative to SMOW. The method also seems to be relatively consistent for this type of analysis; 2 pairs of duplicate samples suggest an analytical precision of ± 3 ‰.

Silicate $\delta^{18}\text{O}$ Analysis

Oxygen isotope analysis within quartz was accomplished by off-line fluorination utilizing the technique established by Borthwick and Harmon (1982). Twenty milligrams of quartz samples were powdered and dried in an oven for 12 hours to remove atmospheric water, and then inserted into nickel reaction vessels. These vessels were evacuated and treated with ClF_3 gas. The samples are first pre-fluorinated with ClF_3 for a period of 10 minutes at room temperature to remove any remaining water, and then heated for eight hours at 450°C with a new aliquot of ClF_3 reagent to produce O_2 gas from the silicate minerals. The O_2 gas was reacted with a carbon electrode to produce CO_2 gas, and then trapped and transferred into sample gas bottles. The yield of O_2 and

CO₂ gases is quantified by Baratron pressure gauges, allowing for percent yield to be calculated. Yields less than 85% are considered unreliable and discarded from the data set. The CO₂ was then analyzed via Dual Inlet against a CO₂ gas standard on a Delta XP IRMS spectrometer for δ¹⁸O. The NBS-28 silica standard was also run with samples to ensure no fractionation was occurring within the silicate line and that values are accurate relative to SMOW. Over the course of analysis, the average measured δ¹⁸O of 5 NBS-28 standards was 9.2 ‰; the known value of the standard is 9.6‰. The analysis of 4 duplicate samples indicates an analytical precision of ± 0.3 ‰. The relatively consistent standard values between runs and high precision allows for the reporting of δ¹⁸O analyses with an accuracy of ± 0.4 ‰ relative to SMOW.

RESULTS

Mineral and Metal Zonation

Using assay information from exploration core provided by Fresnillo PLC, as well as reflected light studies and core logging, it can be shown that the Valdecañas vein exhibits spatial zonation of base and precious metals characterizing epithermal systems (Buchanan, 1981). The greatest concentrations of lead and zinc with only very minor copper, are in the lower portions of the vein, and concentrations tend to decrease in the upper portions of the vein (Figure 4). Conversely, in the topographically higher vein regions, there is an increase in the concentrations of gold and silver. The variable nature of the ore bands is particularly well illustrated by the gold equivalent grades of the vein, expressed in grams/ton (Figure 5).

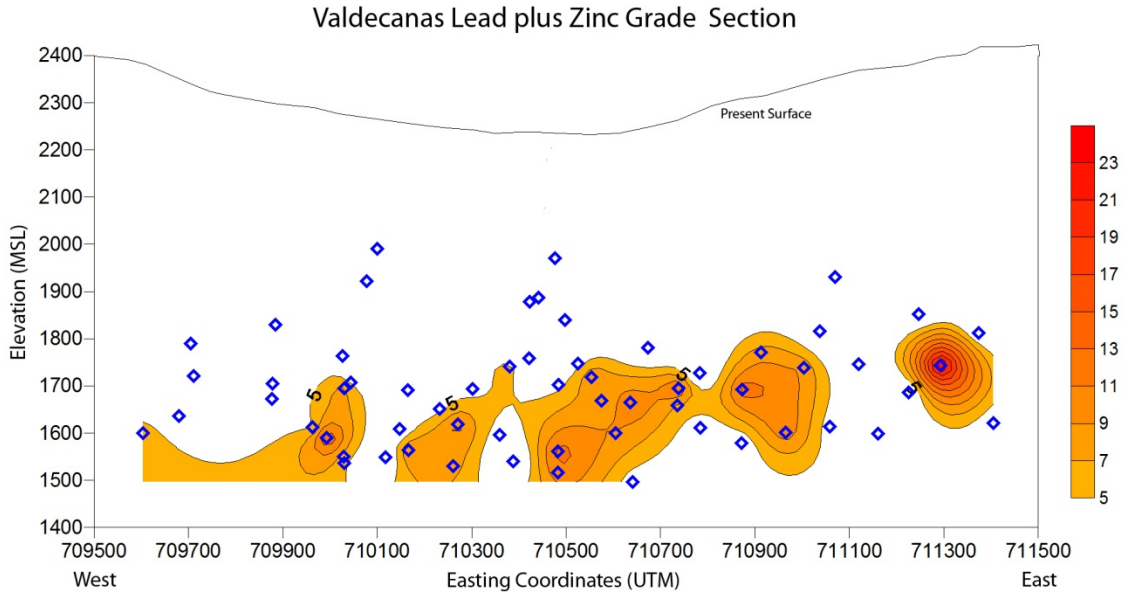


Figure 4. Longitudinal section of the Valdecañas vein, looking north. Blue diamonds represent drill-hole intercepts of the vein. Contours represent Zn+Pb grades (%) from exploration core. White areas represent intercepts with less than 5% total Pb+Zn.

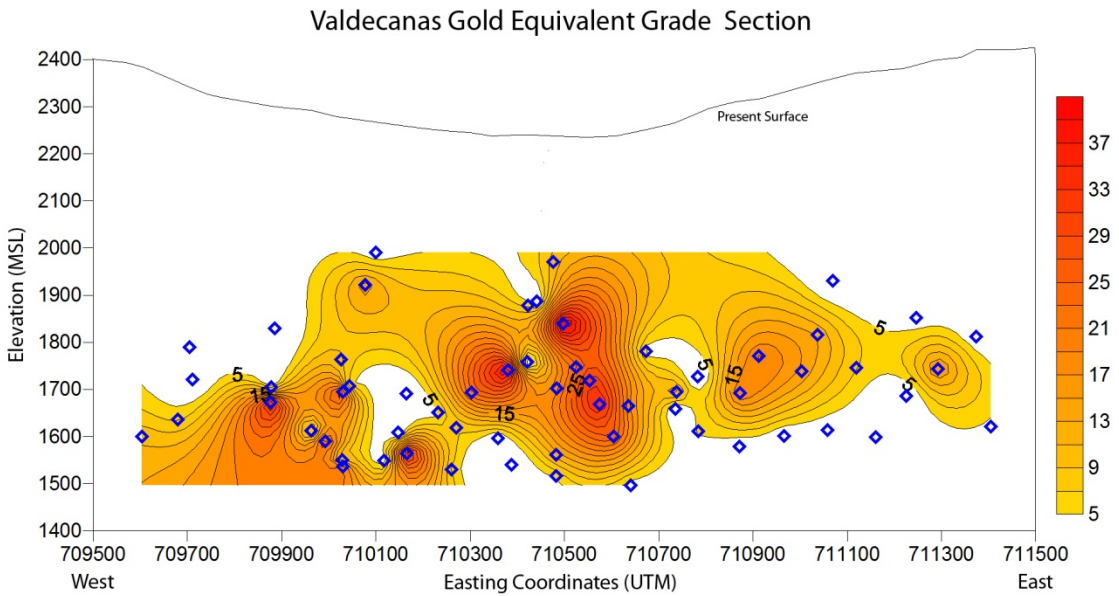


Figure 5. Longitudinal section of the Valdecañas vein, looking north. Contours represent grades of silver and gold in gold equivalent (in grams/ton). Blue diamond represent drill-hole intercepts of the vein. White areas represent intercepts with less than 5 g/ton gold equivalent.

Optical Petrography

Gangue minerals within the vein comprise almost entirely quartz, calcite, and adularia. Several different morphologies of quartz are present, including, coarse grained quartz, medium grained quartz, chalcedonic quartz, and microcrystalline quartz. Coarse grained quartz is typically greater than 20 μ m in diameter and often shows euhedral crystal shape. This type of quartz is present in many sections lining the walls of veins, where it was able to grow into open space (Figure 6A). Medium grained quartz is typically subhedral, and forms within the center portions of veins. Microcrystalline and chalcedonic quartz is also present in all veins, often forming spherical bands and infilling the central portions of quartz and sulfide veins. Calcite has two morphologies—clean, euhedral calcite, and “dirty” calcite that contains small opaque mineral inclusions (possibly sulfides). Adularia, present as euhedral rhombs associated with quartz, occurs in several vein intercepts (Figure 6B).

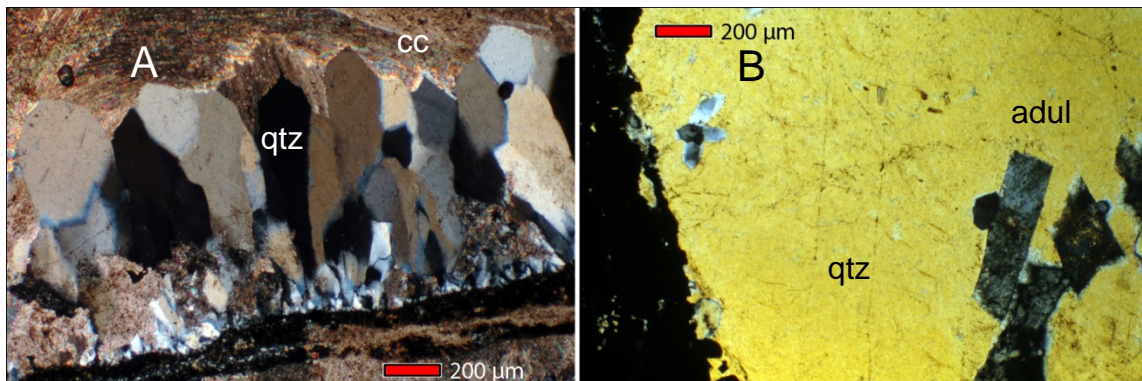


Figure 6. Thin section photomicrographs. A) Large, euhedral quartz crystals with late calcite filling former void space to the outside (Sample GB-02, 728m). B) Large quartz grain (yellow due to thickness of section) with intergrown adularia (adul). (Sample WC-01, 656m).

Sulfide mineralogy is dominated by base metal sulfides, including sphalerite galena, and pyrite. Arsenopyrite is locally present in the upper, western portions of the

vein. Major silver ore minerals are silver sulfosalts, dominated by pyrargyrite. Sphalerite also contains several, probably exsolved, silver-bearing minerals, including acanthite and tennantite/tetrahedrite, with the acanthite present almost exclusively within sphalerite as small exsolved blebs (Figure 7).

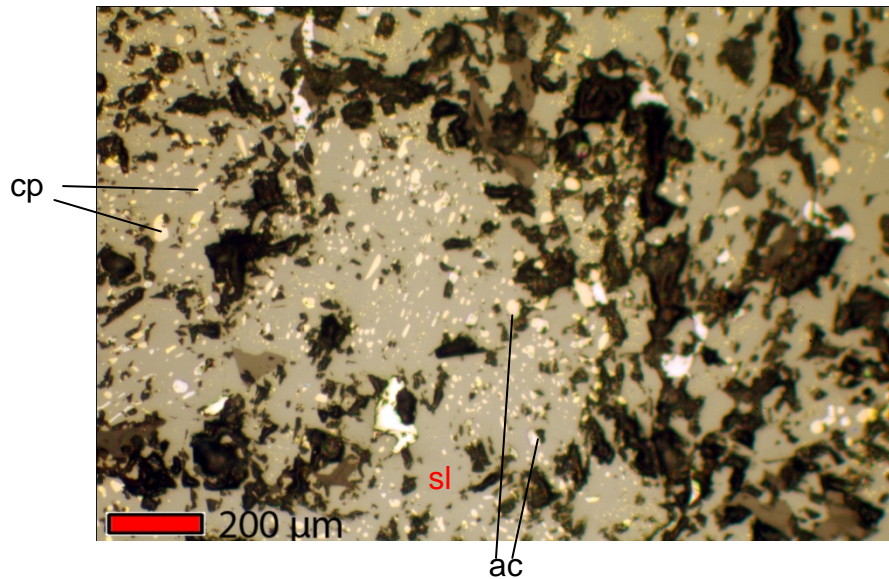


Figure 7. Sphalerite (sl) with exsolved chalcopyrite (cp) and acanthite (ac). Sample (EF-04, 831m)

Paragenesis

The paragenesis of the Valdecañas vein was determined through relationships observed both in hand sample from exploration drill core and from polished thin sections. Results from thin sections examining the small-scale paragenesis from individual samples were compiled and then combined with the results observed from hand samples. Close attention was paid to cross-cutting relationships between the different stages and mineralization events. The following paragenetic scheme (Figure 8) was compiled from these relationships; however, the entire paragenetic sequence is not seen in all portions of the vein. The overall paragenesis of the Valdecañas vein closely resembles the schemes proposed by studies in Fresnillo Southeast by Gemmell et al. (1988) and Dilley (1993)

(the Santo Niño and San Mateo Veins, respectively), as well as the Jarillas vein studied in Fresnillo Southwest by Velador (2010).

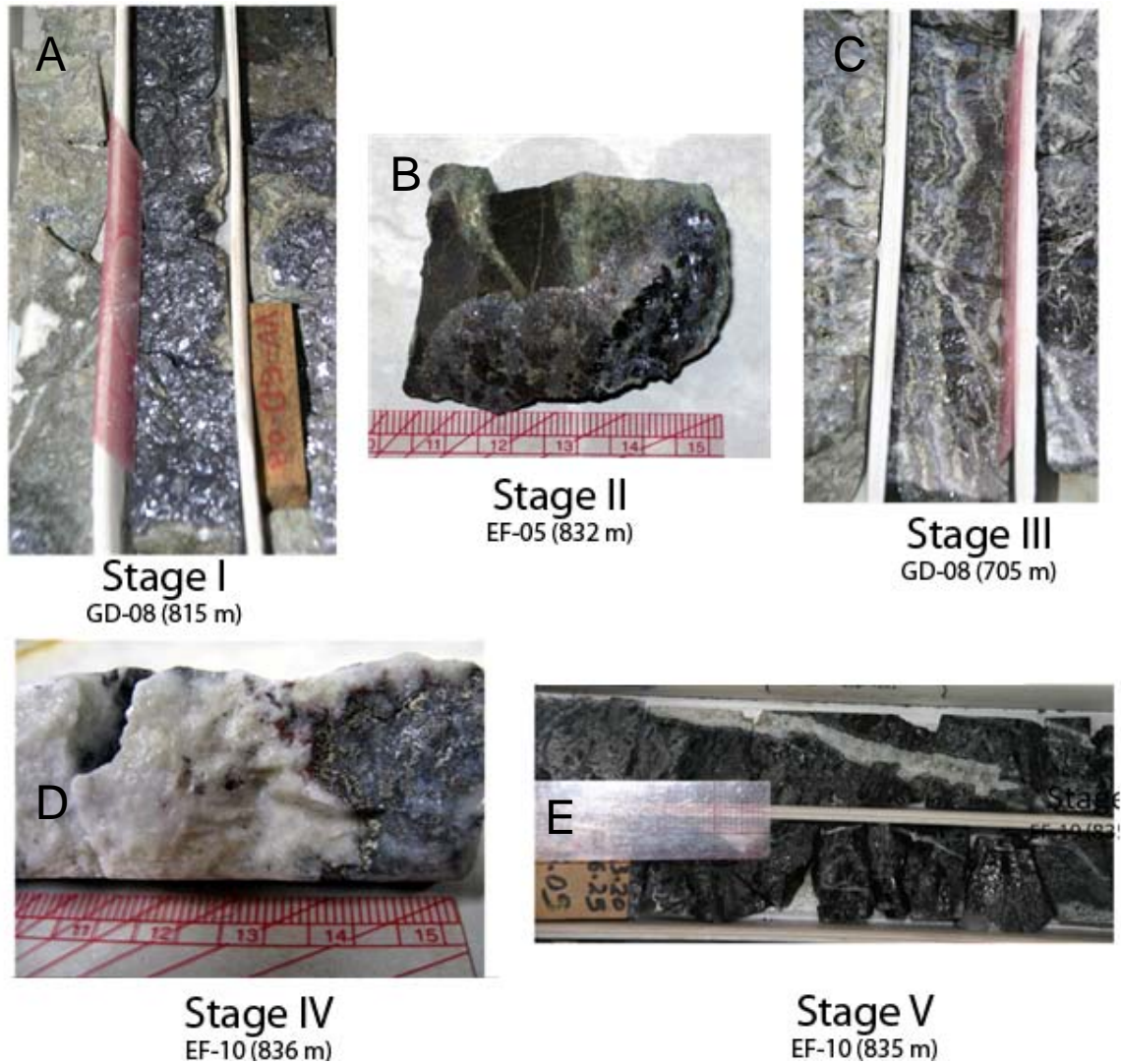


Figure 8. Different mineralizing stages within the Valdecañas vein. A) *Stage I*. Coarse sphalerite and galena developed from local wall rock. B) *Stage II*. Brecciation of coarse sulfides and infilling of quartz and calcite. C) *Stage III*. Main ore stage, with thin crustiform bands of quartz and sulfides. D) *Stage IV*. Calcite with visible pyrrargyrite (red) E) *Stage V*. Coarse quartz and calcite with only minor sulfides present as pyrite.

Stage I This stage is characterized by the brecciation of wallrock and infilling by coarse base metal sulfides. Massive galena and sphalerite dominate this stage of mineralization,

with minor chalcopyrite occurring near the end of the stage. This stage is almost always in direct contact with Guerrero wallrock, either deposited along fractures within the rock itself or surrounding and infilling brecciated host rock fragments. These relationships are present in the GD (815-816m, Figure 8a) and MF (816-817m) drill cores.

Stage II This stage is characterized by the brecciation of the massive sulfides of *Stage I*, and the infilling by fine, greenish quartz, with minor calcite around *Stage I* clasts. Sample EF-05 (832m) (Figure 8b) exemplifies relationships seen within the core samples. In this sample, a large fragment of coarse galena and sphalerite attached to the Guerrero wallrock has been fragmented and cemented by greenish quartz.

Stage III This stage is the principal ore stage of deposition, characterized by fine, crustiform bands of quartz and calcite with sulfides. Sulfides are dominated by pyrite, arsenopyrite, sphalerite, galena, and silver sulfosalts, with local chalcopyrite (Figure 8c). This stage of mineralization often cuts the greenish quartz and calcite from Stage II, as seen in the QF exploration drill core (QF-4, 623m).

Stage IV The fourth stage is dominated by calcite, that cross-cuts the banded sulfides of earlier stages. Sample EF-10 (836m, Figure 8d), exemplifies this relationship, where a large, coarse calcite vein with fine pyrargyrite cuts a banded vein of quartz, pyrite, and sphalerite minerals from *Stage III*. This stage frequently contains coarse-grained pyrargyrite and minor disseminated pyrite. Base metal sulfides are not present.

Stage V A continuation of *Stage IV*, this stage consists of barren coarse quartz and calcite, but lacks any base metals or silver-bearing minerals. Disseminated pyrite is sometimes present within this stage, but only comprises a very minor portion of the veins. These veins are found cutting *Stage III* veins within several drill core vein intercepts,

including the EE hole (772-773m). *Stage V* veins also directly cut *Stage I* sulfides (OF-6, 795m) and the Guerrero hostrock on the fringes of large vein intercepts (Figure 8e).

The paragenetic relations are summarized in Figure 9.

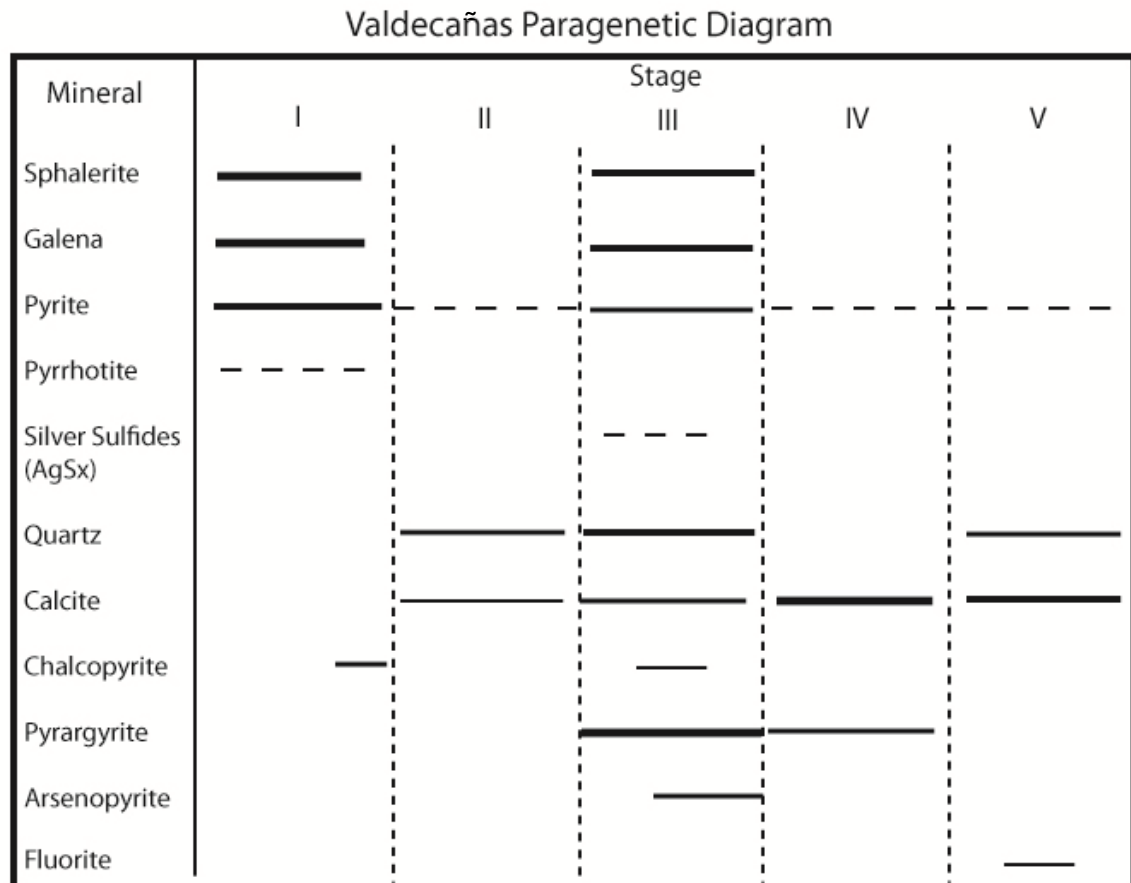


Figure 9. Paragenetic diagram of minerals within the Valdecañas vein. *Stage III* represents the main stage of ore deposition, with subordinate silver and important base metals in *Stage IV* and *Stage I*, respectively.

Fluid Inclusions

In this study, 265 inclusions within quartz and 76 inclusions within calcite were analyzed, producing 341 homogenization temperatures and 334 melting point depressions. The majority of inclusions (265) were measured from quartz and calcite

bands within the *Stage III* Ore stage; 65 late quartz and calcite inclusions from *Stage V* were also measured.

Inclusion Types

Measured fluid inclusions within the sections range in size from 4-25 μm in diameter, with an average size of 8 μm . Two types of inclusions exist within the samples; liquid-vapor (L-V) inclusions with over 50% liquid, and vapor-dominated inclusions. L-V inclusions compose over 99% of all observed inclusions. Primary, pseudo-secondary, and secondary inclusions were observed and measured. The classification of inclusions into these groups was accomplished by physical relationships and morphologies, and utilized the scheme proposed by (Roedder, 1984). Vapor-dominant inclusions were observed in close proximity to L-V inclusions in many sections, which is evidence for boiling within the system (Roedder, 1984).

Microthermometry

Fluid inclusion temperatures for the Valdecañas vein range from 160 to 320°C, with an average temperature of 248°C and a modal temperature of approximately 260°C (Figure 10). Salinities range from 0 to 11 wt.% NaCl equivalent, with an average salinity of 3.7 wt. % and a modal salinity of 2.5 wt. % NaCl equivalent (Figure 11).

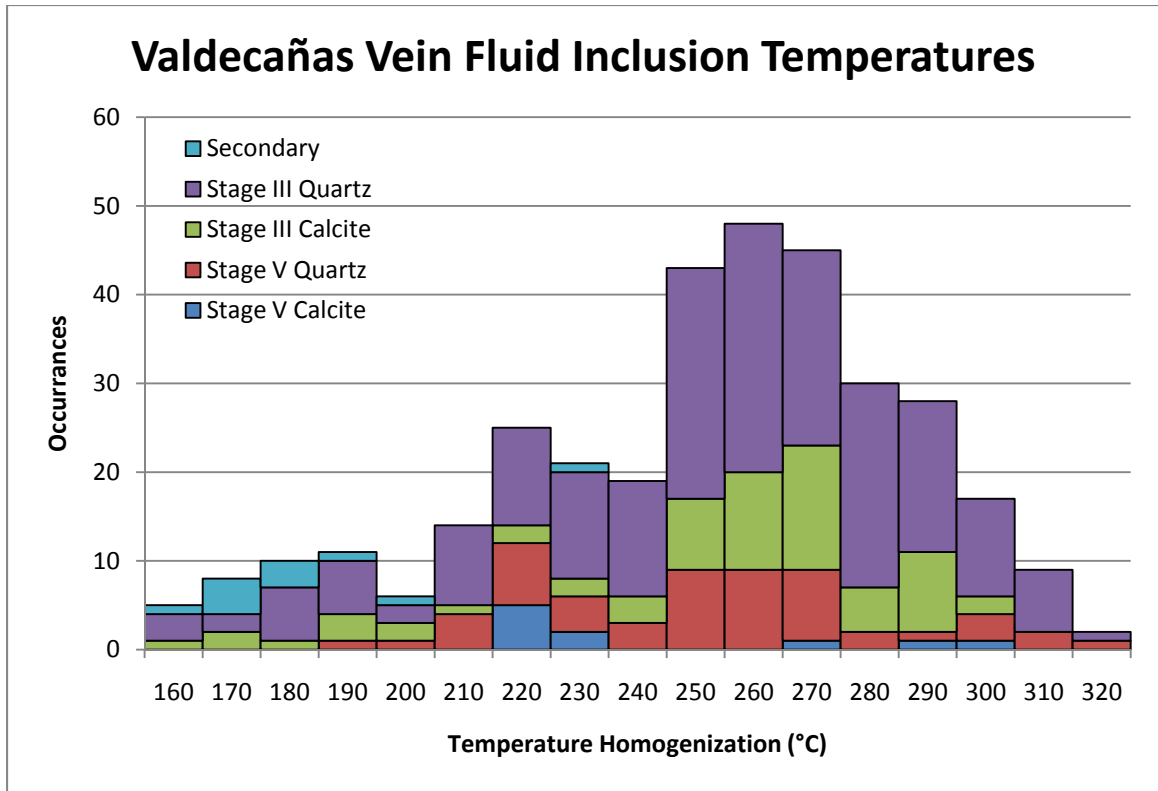


Figure 10. Fluid inclusion temperatures of homogenization for the Valdecañas Vein. *Stage III* represents the main ore stage of mineralization.

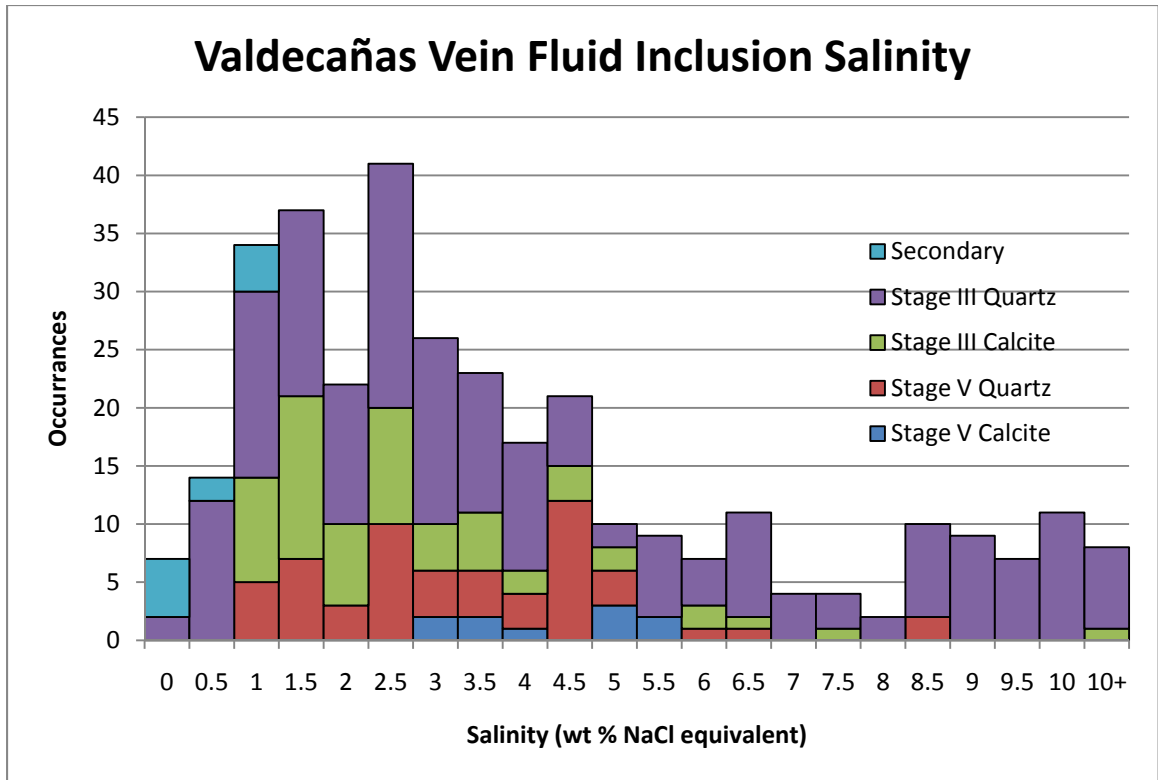


Figure 11. Calculated salinities (from melting point depression measurements) computed from the equations of Bodnar (1993).

Stable Isotopes

Sulfur Isotopes

Sulfur isotope analysis for $\delta^{34}\text{S}$ was performed on 121 mineral separates from 72 samples spanning five veins within the Fresnillo Southwest district. The majority of the samples (64) were taken from the Valdecañas vein system, which was the focus of the study (Figure 12). The remainder were taken from the Jarillas (39), Santa Natalia (2), San Diego (11), and Saucito (4) (Figure 12). From each sample, pyrite, galena, sphalerite, or chalcopyrite separates were analyzed. One sedimentary pyrite nodule from the Guerrero terrain sedimentary unit was also collected from a drill core that did not intercept any of the exploration veins, and was analyzed to establish a sedimentary pyrite

$\delta^{34}\text{S}$ value. Sulfur from mineral analyses and calculated H_2S values from the mineral analyses using fluid inclusion temperatures are reported in Table 1.

Table 1. Mineral $\delta^{34}\text{S}$ values from veins within Fresnillo Southwest.

Vein	Sulfide Mineral Separates (‰, vs. CDT)							F.I. Temp (°C)	Calculated H_2S $\delta^{34}\text{S}$ Values ‰		
	Py	Gn	Sl	Cpy	Aspy	Po	Pyrar		Py	Gn	Sl
Jarillas Vein											
JV-F8-02			-4.1			-4.6		230			-4.5
JV-FS95-1	-5.0	-6.5						230	-6.5	-4.0	
JV-G5-5					-6.8			260			
JV-G5-6		-6.2						260		-4.0	
JV-G5-9	-4.8							260	-6.2		
JV-G7-13			-6.3					250			-6.6
JV-G7-3	-4.9		-4.7					250	-6.4		-5.0
JV-G7-5			-5.0					250			-5.4
JV-G7-6			-5.2					250			-5.6
JV-G7-8			-5.9				-6.4	250			-6.3
JV-G9-7			-5.7					255			
JV-G9-8		-8.3	-5.8					255		-6.1	-6.1
JV-H11-3	-5.3		-4.8					250	-6.8		-5.2
JV-I9-6	-3.6		-4.4					250	-5.1		-4.8
JV-K7-02			-4.1					235			-4.5
JV-K7-11		-6.9	-4.4					235		-4.5	-4.8
JV-K9-12		-9.2	-6.8					235		-6.8	-7.2
Jv-M11-1			-5.5					220			-5.9
JV-Q11-1		-5.8		-4.3				230		-3.3	
JV-Q11-6	-3.1	-5.7	-4.4					230	-4.7	-3.2	-4.8
JV-Q9-1	-3.7	-6.5						230	-5.3	-4.0	
JV-Q9-4			-4.2					230			-4.6
JV-S7-03-1	-4.1	-6.3						240	-5.6	-3.9	
JV-S7-03-2	-4.2							240	-5.7		
San Carlos Vein											
VSC-R8-1							-3.6				
San Diego Vein											
SD-1138-2	-1.3	-5.7						240	-2.8	-3.3	

SD-1140-1			-4.7					240			-5.1
SD-1145-1		-8.7	-5.0					240		-6.4	-5.4
SD-1145-2	-6.1	-7.1	-7.2					240	-7.6	-4.8	-7.6
SD-1145-3	-5.3							240	-6.8		
SD-1146-2	-4.3		-3.9			-3.6		240	-5.8		-4.2
Santa Natalia Vein											
SN-1140-1	-7.4							240	-8.9		
SN-1143-1			-3.8					240			-4.2
Saucito Vein											
VS-38F-1	-6.1							240	-7.6		
VS-38F-2	-5.1							240	-6.6		
VS-FS13-1	-4.0							240	-5.5		
VS-FS14-2	-4.2							240	-5.7		
Valdecañas Vein											
VV-13P-2			-3.7					260			-4.0
VV-13P-3	-5.8	-8.4						260	-7.2	-6.2	
VV-16P-2	-4.9	-6.3	-3.8					260	-6.3	-4.1	-4.1
VV-16P-3	-4.7		-4.3					260	-6.2		-4.7
VV-GD-01			-4.4					260			-4.8
VV-GD-02	-4.8		-5.1					287	-6.1		-5.5
VV-GD-04	-2.7	-6.0	-4.0	-5.3				280	-4.0	-3.9	-4.3
VV-GD-05			-3.8					280			-4.1
VV-GD-07		-6.6						280		-4.5	
VV-GD-07			-5.4					280			-5.8
VV-GD-08		-5.7	-4.5					280		-3.7	-4.8
VV-GD-10	-5.4		-4.5					280	-6.7		-4.8
VV-GD-11		-7.3	-4.8					280		-5.2	-5.1
VV-GD-12			-5.3					280			-5.6
VV-MF-3	-5.3	-7.4						257	-6.7	-5.2	
VV-MF-5	-5.8		-4.6					257	-7.2		-5.0
VV-MF-6	-6.0	-7.0	-4.3					257	-7.4	-4.7	-4.6
VV-MF-7	-4.2							257	-5.6		
VV-SD-2			-4.4					257			-4.8
VV-SD-3	-3.5		-4.5					257	-5.0		-4.8
VV-QF-7	-1.6	-6.8	-4.4					285	-2.8	-4.7	-4.7
VV-EE-7	-4.6	-6.7	-4.6					265	-6.0	-4.5	-4.9
VV-ME-05	-4.1	-6.6						260	-5.5	-4.4	
VV-OF-3	-5.6	-7.0	-5.5					275	-6.9	-4.9	-5.8
VV-OF-1	-5.6							275	-6.9		
VV-GB-05		-7.4						250		-5.1	

VV-GB-03			-5.4					250			-5.8
VV-UD-08		-7.3		-5.2				260		-5.1	
VV-EF-04	-4.1							260	-5.5		
VV-EF-02	-4.1		-4.0					260	-5.5		-4.3
VV-KD-08			-3.9					260			-4.3
VV-KD-10	-5.1	-7.0						260	-6.5	-4.8	
VV-ME-02	-3.3	-6.4	-3.9					260	-4.7	-4.2	-4.2
VV-WC-01	-2.9							260	-4.3		
VV-WC-01				-4.3				260			
VV-WC-03		-7.2						260		-5.0	
VV-ME-1							-20.8	275			
Guerrero Terrain Sediments											
Sed. Pyrite	-26.4										

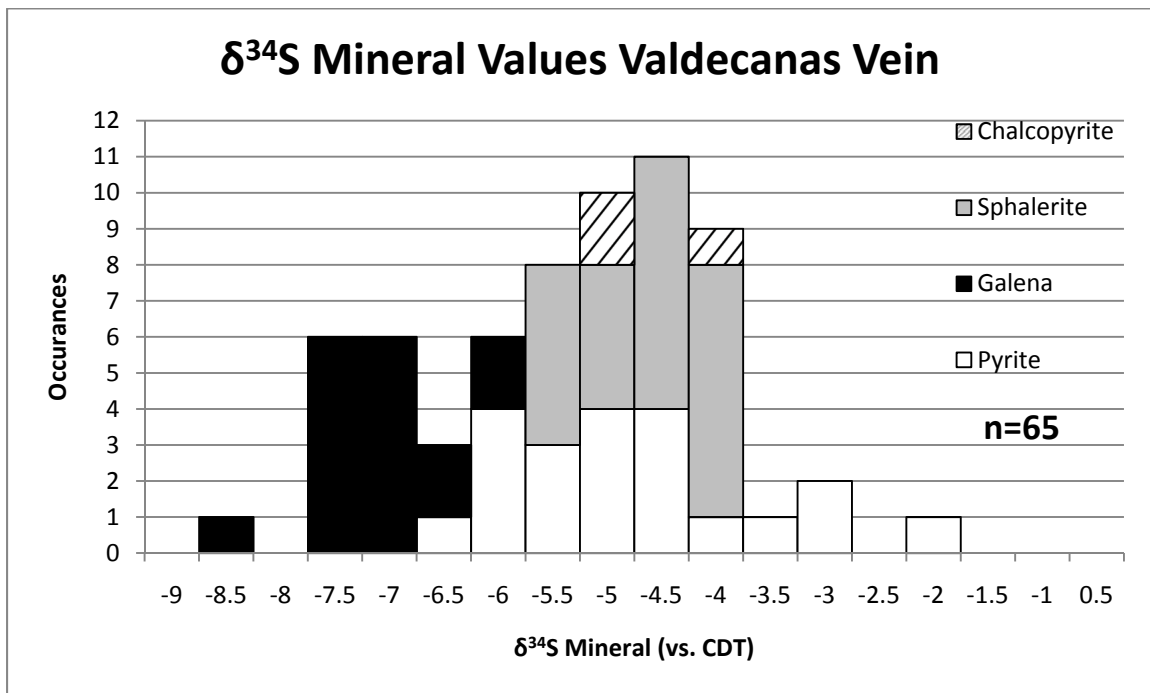


Figure 12. Histogram of $\delta^{34}\text{S}$ values from different minerals within the Valdecañas vein.

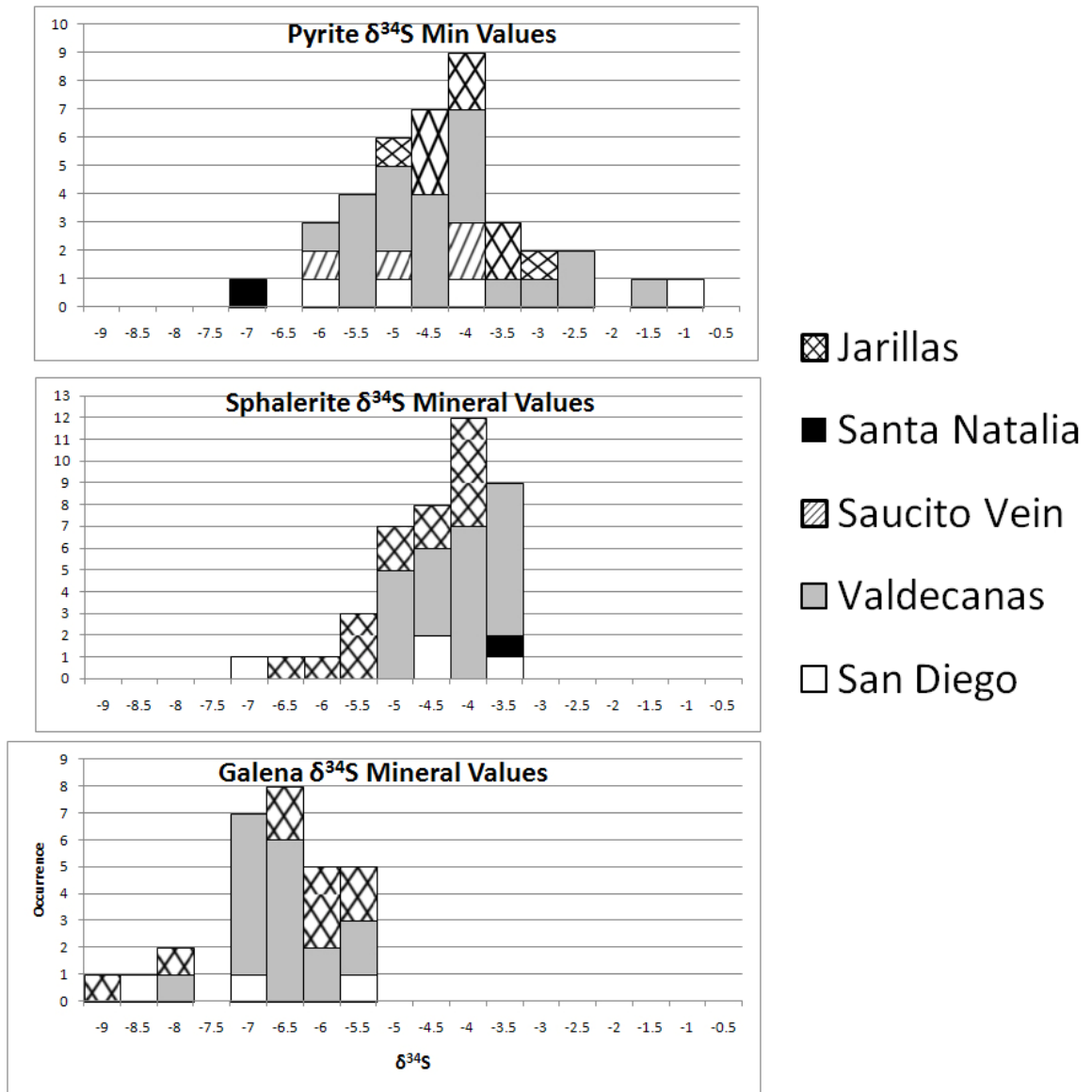


Figure 13. Histogram representing distribution of aqueous H_2S $\delta^{34}\text{S}$ values from five veins in the Fresnillo Southwest district

Carbon, Oxygen, and Hydrogen Isotopes

The carbon isotope values from 13 calcite separates are summarized on Table 2.

Ten of the 13 samples were taken from *Stage III* calcite, one sample was taken from *Stage IV*, and the remaining two were from late *Stage V* calcite. The values fall within a

relatively narrow range of -9 to -7 ‰, with the exception of one late calcite sample that has a $\delta^{13}\text{C}$ value of -4 ‰.

The calcite mineral separates as well as nine quartz mineral separates from the Valdecañas vein were analyzed for $\delta^{18}\text{O}$. Six of these same quartz samples were analyzed for fluid inclusion δD . The oxygen, hydrogen, and carbon isotope values from these minerals are summarized in Table 2.

Table 2. $\delta^{18}\text{O}$, δD , and $\delta^{13}\text{C}$ values from the Valdecañas vein.

Sample	Stage	Cc Min. Values		Qtz Min. Values	F.I. δD	F.I. Th	Cc $\delta^{18}\text{O}$ H ₂ O	Qtz $\delta^{18}\text{O}$ H ₂ O
		$\delta^{13}\text{C}$	$\delta^{18}\text{O}$	$\delta^{18}\text{O}$		°C		
EE-06	III			16.3	-63	265		9.02
EE-10	III	-7.5	9.7	15.4		265	8.6	
EF-08A	III	-7.0	12.2	12.5		260	10.8	
EF-09	V	-4.0	12.8			257	11.2	
EF-10	IV	-7.0	8.9			257	7.3	
GB-04	III	-8.3	10.4			250	8.4	
GD-02	III			16.8	-69	287		10.6
GD-04	III	-9.1	9.3			280	9.2	
KD-05	III	-8.2	10.6			260	9.2	
KD-08	III	-8.1	8.8			260	7.4	
KD-09	III			14.0		260		6.5
ME-02	III	-7.8	8.9			260	7.6	
OF-1	III	-7.0	8.8	14.5	-57	275	8.3	7.7
QF-4	III	-7.0	8.7			285	8.8	
QF-9	V	-8.0	7.4	12.4		262	6.2	5.0
UD-01	III	-8.1	12.9	14.9	-54	260	11.5	7.4
WC-02	III			15.3	-79	260		7.8

INTERPRETATIONS

Fluid Inclusions

Homogenization temperatures seem to be very consistent between *Stage III* and *Stage V* inclusions (Figure 14). The temperature ranges of the two stages overlap each other completely, and have the same modal temperatures. There does seem to be slightly

higher salinity within stage III quartz and calcite inclusions. This suggests that the fluid might have become slightly less saline over time, although Th values seem show the same variability within the two different stages. Secondary inclusions do show a distinct grouping at lower temperatures, and contain almost zero salinity, suggesting that the fluids moving through the vein deposits were cooler and contained lower salinities at later times in the vein's history.

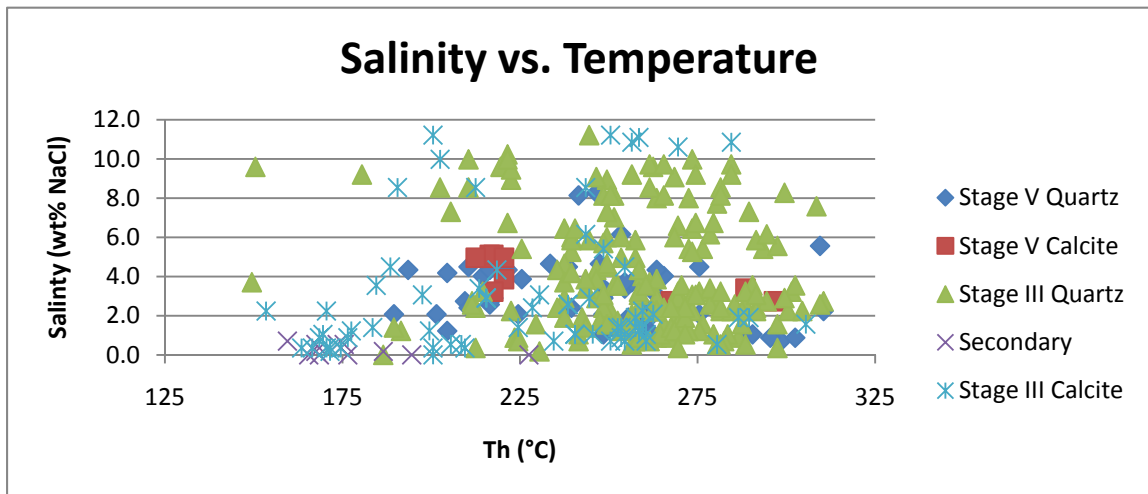


Figure 14. Salinity versus homogenization temperature diagram of measured inclusions within the Valdecañas vein.

To visualize the spatial relationship of inclusions, histograms of homogenization temperatures and salinity for each drill hole intercept were compiled (Figures 15, 16).

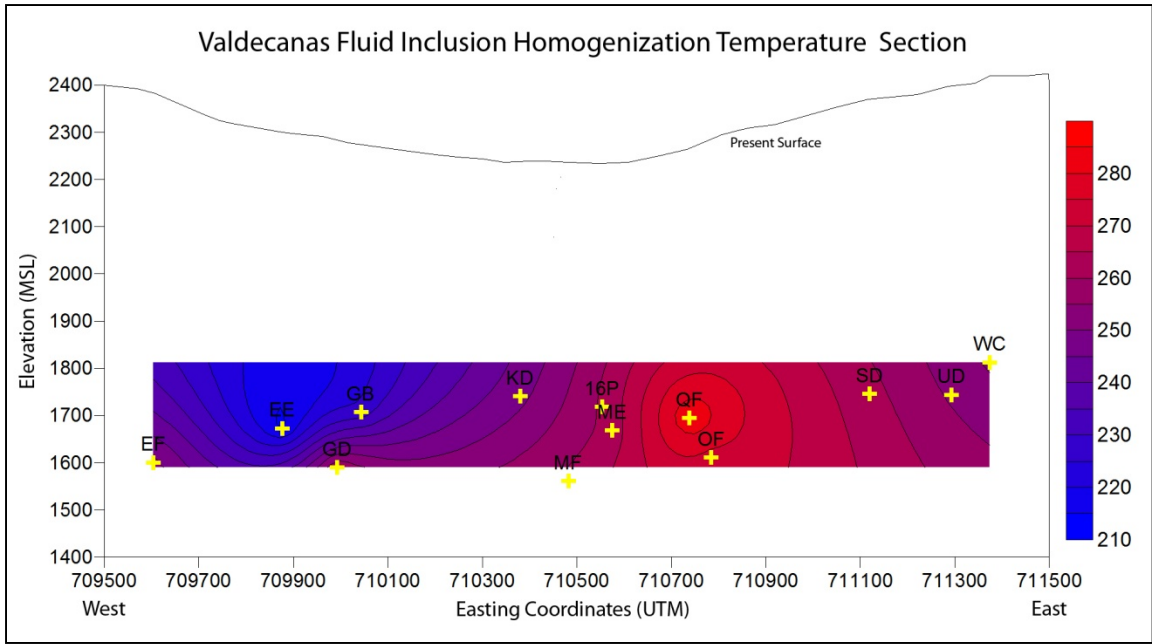


Figure 15. Longitudinal section of Valdecañas vein showing sampled drill intercepts and homogenization temperature gradient. Red shadings are hot (maximum T of 285°C), blue shading are lower temperatures (minimum T of 210°C). Drill intercepts QF and OF show the highest homogenization temperatures.

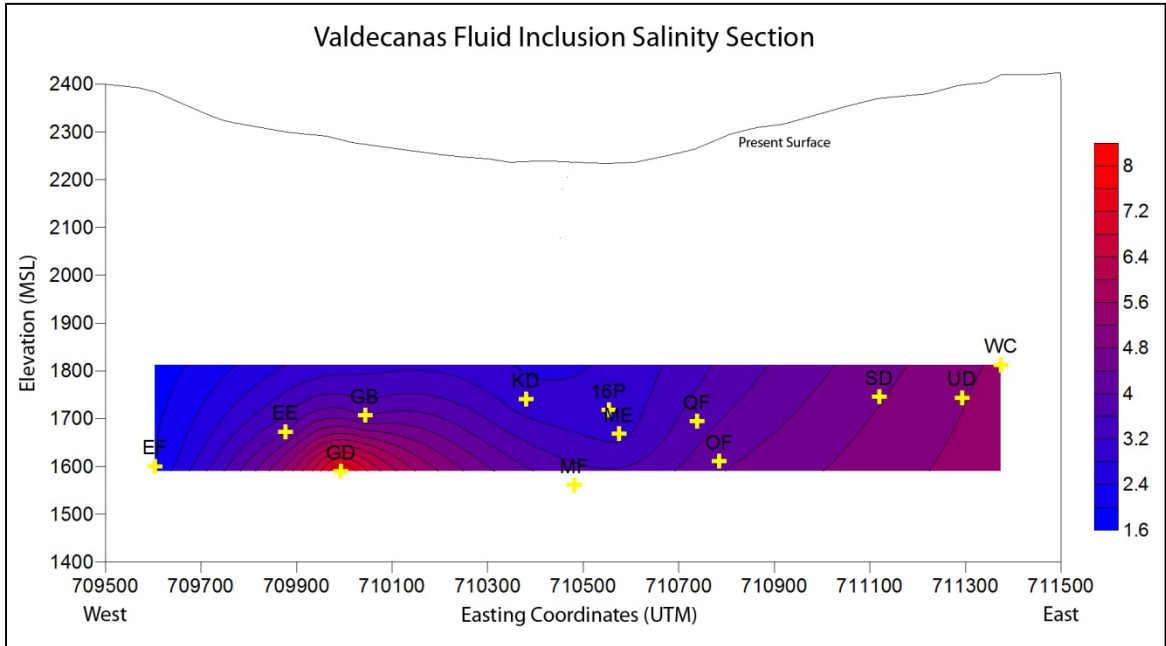


Figure 16. Longitudinal section of Valdecañas vein showing sampled drill intercepts and fluid inclusion salinities. Red shadings are highest salinities (maximum of 8 % NaCl eq.), blue shading are lower (minimum of 1.5 % NaCl eq.)

The highest homogenization temperatures were measured from the west central portion of the Valdecañas vein. Salinity is much less defined, but it is evident that the areas with highest salinity do not correspond with high temperatures. The east-central portion of the vein with the highest homogenization temperatures is interpreted to represent the conduit where fluids migrated upwards into the system.

Stable Isotope Geothermometry

Sulfide Minerals

Petrographic relationships between sphalerite and galena within the Valdecañas veins suggest the minerals are cogenetic and thus formed from the same ore fluid.

Geothermometry calculations on sphalerite-galena pairs from several samples from the Valdecañas and Jarillas veins were performed using the fractionation factors presented by Ohmoto and Rye (1979).

The results of the geothermometry are varied; although many samples produced realistic temperatures, a substantial number produced unrealistic temperatures (less than 100°C), suggesting the galena and sphalerite minerals were not an equilibrium assemblage. Nonetheless, the temperatures derived from separates drilled from the same billet (millimeter separation) are relatively consistent with temperatures determined by fluid inclusion microthermometry (Table 3), and support the petrographic observations indicating these minerals to be cogenetic. However, samples selected from different portions of hand samples (centimeter separation) produce anomalously low temperatures. This suggests that sphalerite and galena minerals not immediately adjacent are not cogenetic, and were precipitated from different pulses of fluid with different

temperatures, or from aqueous H₂S with slightly different $\delta^{34}\text{S}$ values. The results suggest that $\delta^{34}\text{S}$ analysis of sphalerite-galena mineral pairs located within very close proximity function well as a means of determining ore temperatures within the Valdecañas vein, and potentially the entire Fresnillo district, despite the overall variations in determined temperatures.

Table 3. Stable isotope geothermometry of sphalerite-galena and quartz-calcite mineral pairs within the Valdecañas and Jarillas veins.

Vein	Sample	F.I. Th	Sphalerite-Galena Pair Temp. (°C)		Quartz-Calcite Pairs
			Drilled	Picked	
Valdecañas Vein					
	VV-QF-7	285	284		
	VV-EE-7	267	318		
	VV-GD-04	280	328		
	VV-ME-02	260	270		
	VV-OF-3	302	414		
	VV-GD-11			66	
	VV-GD-08			58	
	VV-GD-07			339	
	VV-MF-6			43	
	VV-QF-9	289			36
	VV-EE-10	265			16
	VV-EF-08A	287			896
	VV-OF-1	275			15
	VV-UD-01	287			214
Jarillas Vein					
	JV-Q11-6	230		491	
	JV-K7-11	235		269	
	JV-G9-8	255		262	
	JV-K9-12	235		274	

Quartz and Carbonate

Quartz and calcite often appeared texturally cogenetic, but proved to be relatively unreliable as geothermometers. This could be a result of poorly selected, intergrown samples that might have been deposited at different times from evolving fluids, or contamination of the calcite by other carbonate minerals that would influence the fractionation factors.

Sulfur Isotopes

Calculated $\delta^{34}\text{S}$ values of $\text{H}_2\text{S}_{(\text{aq})}$ were determined from the mineral values and the appropriate temperatures taken from the modal Th value for that sample where available. Th values from the Santa Natalia, San Diego, and Saucito were not available, so the average temperatures from the Valdecañas and Jarillas veins were assumed for these veins based on the similar mineral paragenesis, depths, and host rock within these veins. To determine whether the fluids were H_2S -dominated, gas analysis data from the Valdecañas and Jarillas veins from Velador (2010) was used to calculate the oxygen fugacity of the system.

Using concentrations of gases such as H_2 and CH_4 from fluid inclusions within the Valdecañas vein, $f\text{O}_2$ can be calculated using thermodynamic equilibrium equations. Within Valdecañas, $\log f\text{O}_2$ ranges from -42 to -35, with an average of -39. Assuming acidic to neutral pH environments, which are typical of intermediate to low-sulfidation systems (Hedenquist et al., 2000; Sillitoe and Hedenquist, 2003), this range of values suggests a reducing environment where the dominant sulfide species in solution would be H_2S (Figure 17). These values are consistent with data from previous studies by Benton

(1993), who analyzed gas from fluid inclusions of the Santo Niño vein and obtained oxygen fugacities ranging from -40 to -38 (log fO_2). It can therefore be concluded that reducing conditions were present throughout much of the Fresnillo system during base and precious metal deposition, and are much lower than what is expected within intermediate sulfidation systems (Hedenquist et al., 2001). The presence of reducing fluids at Fresnillo is supported by the lack of any observed sulfate minerals within the veins, and by the fact that the sedimentary host rocks at Fresnillo contain reduced, black shales which reasonably would have influenced ore fluid chemistry via buffering. After determining the chemistry and bulk speciation of sulfur in the fluids, the temperature information obtained from fluid inclusions was utilized in conjunction with the sulfide- H_2S fractionation equations published by (Ohmoto and Rye, 1979) to determine the bulk $\delta^{34}S$ of the ore-forming fluid.

The mineral and fluid H_2S $\delta^{34}S$ values from vein to vein, as well as from early to later stages of sulfide deposition, are remarkably consistent (Figure 18). This is especially true for sphalerite and galena fluid values, which show a very tight grouping around -4.5 to -6‰. This suggests these minerals formed from the same fluid, which did not fluctuate in composition significantly over the period of base metal deposition. The pyrite exhibits a larger spread of values, forming from fluids ranging in $\delta^{34}S$ from -7 to -2‰; these wider values could be explained by larger fluctuations in fluid temperature or composition during pyrite deposition, although the $\delta^{34}S$ distribution within analyzed samples does not seem to have any relationship to earlier or later pyrite separates from different stages of mineralization.

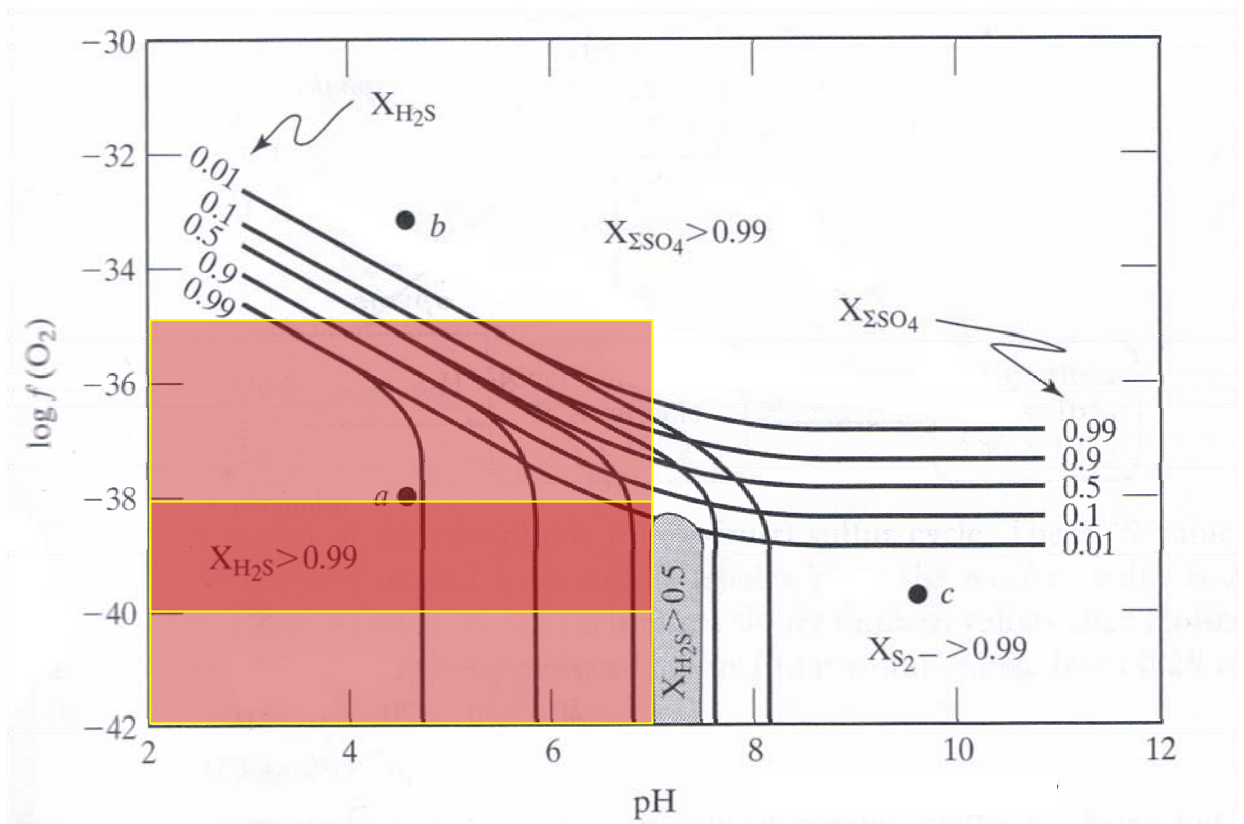


Figure 17. Diagram showing aqueous sulfur species at different pH and oxygen fugacities. Red shaded area represents gas analysis values from Velador (2010). Darker shaded area represents values from Benton (1991) from the Santo Niño vein, and encompasses the average values from Valdecañas. Diagram modified from Sharp (2007).

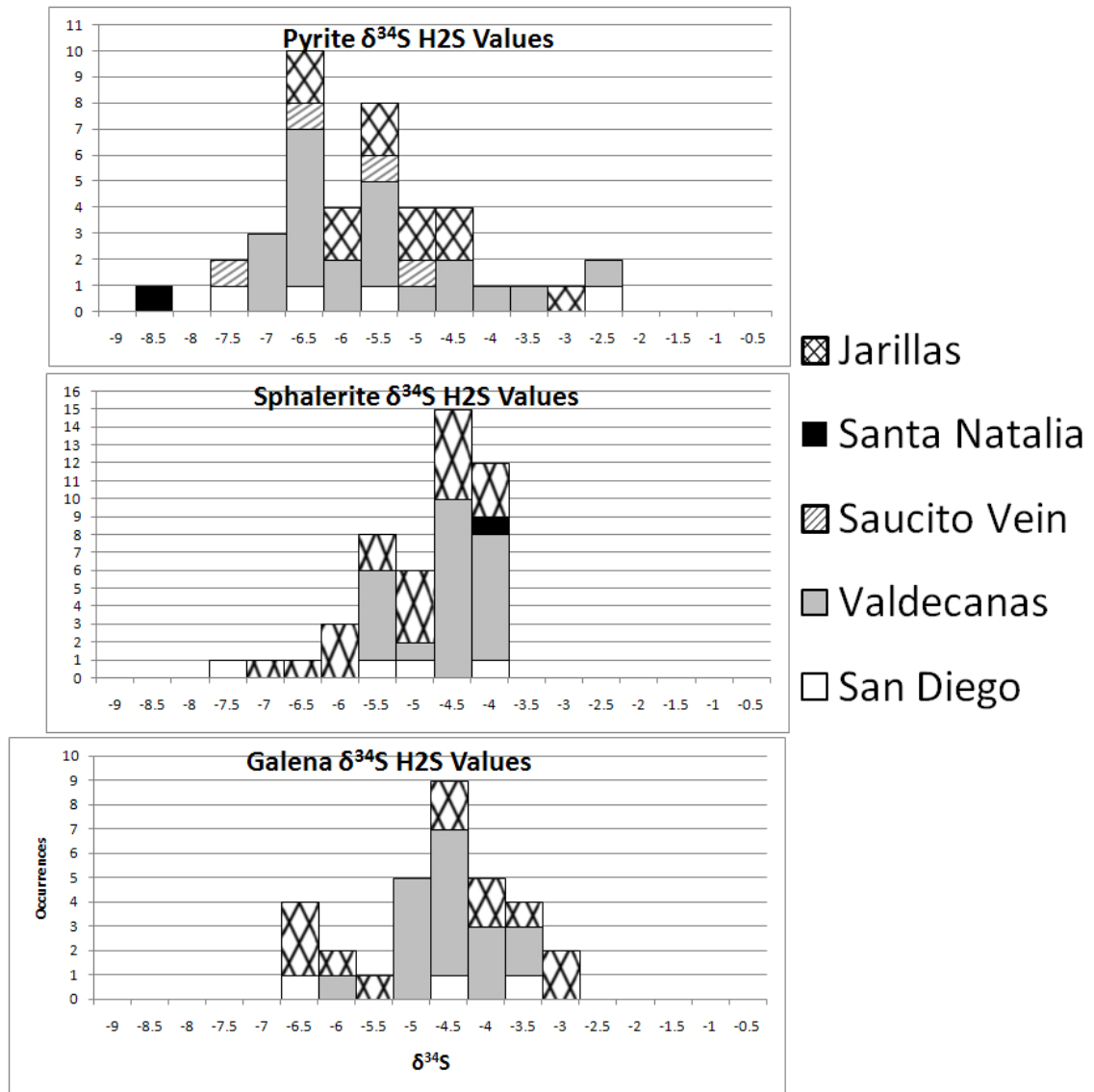


Figure 18. Histograms of calculated H₂S values from pyrite, sphalerite, and galena from several different veins within Fresnillo Southwest.

Carbon, Oxygen, and Hydrogen Isotopes

The values from the calcite and silicate minerals show no major fluctuations over the entire span of the Valdecañas vein. Fluid values from carbonate and quartz minerals were calculated using the fractionation equations from Kim and O’Neil (1997) and Meheut et al. (2007) respectively, with temperatures determined from fluid inclusion

analysis. The resulting $\delta^{18}\text{O}$ values of water calculated from samples containing both calcite and quartz vary significantly; waters calculated from calcite were consistently heavier (up to 3 ‰) than waters calculated from quartz. This suggests these minerals were not in equilibrium, which is evidenced by the poor geothermometry results obtained when using the mineral pairs. This disequilibrium could be a result of the minerals depositing at different times (with different temperature conditions), or the incorporation of heavy carbonate (CO_3^{2-}) from the sedimentary host rocks. The heavier, sedimentary carbonate, assuming it is out of equilibrium with the ore-forming fluids, would represent heavier water than what was present in the system depositing quartz.

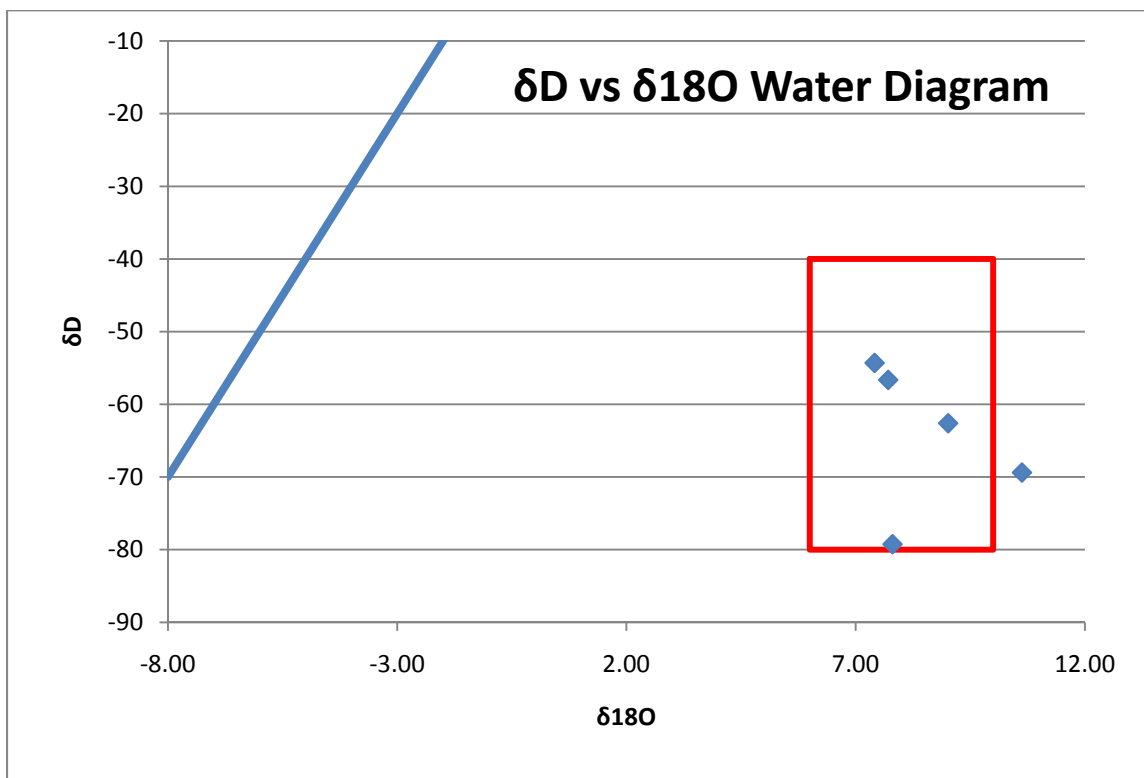


Figure 19. δD vs. $\delta^{18}\text{O}$ diagram of water calculated from quartz mineral values and fluid inclusion water. Red box represents the magmatic water box; blue line represents the modern-day meteoric water line.

The calculated water compositions from paired quartz and fluid inclusion analyses all fall within or near the magmatic water box, similar to results reported in previous studies by (Benton, 1991; Simmons et al., 1988). These results could be interpreted as magmatic water released from intrusions, highly exchanged meteoric waters, or a mixture of both. The Guerrero Terrane in the Fresnillo area contains abundant carbonate sediments that could exchange the oxygen within meteoric waters to reflect the heavy values seen in the Valdecañas vein samples.

The $\delta^{13}\text{C}$ values from calcite cannot provide much definitive information on the source of carbon in the system. The range of $\delta^{13}\text{C}$ values could be attributed to several different sources of carbon, including magmatic as well as sedimentary and organic carbonate sources (Sharp, 2007). When combined with the carbonate mineral $\delta^{18}\text{O}$ values (Figure 20), the majority of the samples plot within the magmatic carbon box defined by (Sharp, 2007). Assuming the oxygen within the carbonate minerals is representative of the original source, and not influenced by the ore forming fluids itself, it can be surmised that the carbonate within Fresnillo was derived from a magmatic source. However, the values that fall to the right of the box, with heavier oxygen values, could represent carbonate incorporated from sedimentary units, which would be expected to contain heavier $\delta^{18}\text{O}$ values (Sharp, 2007).

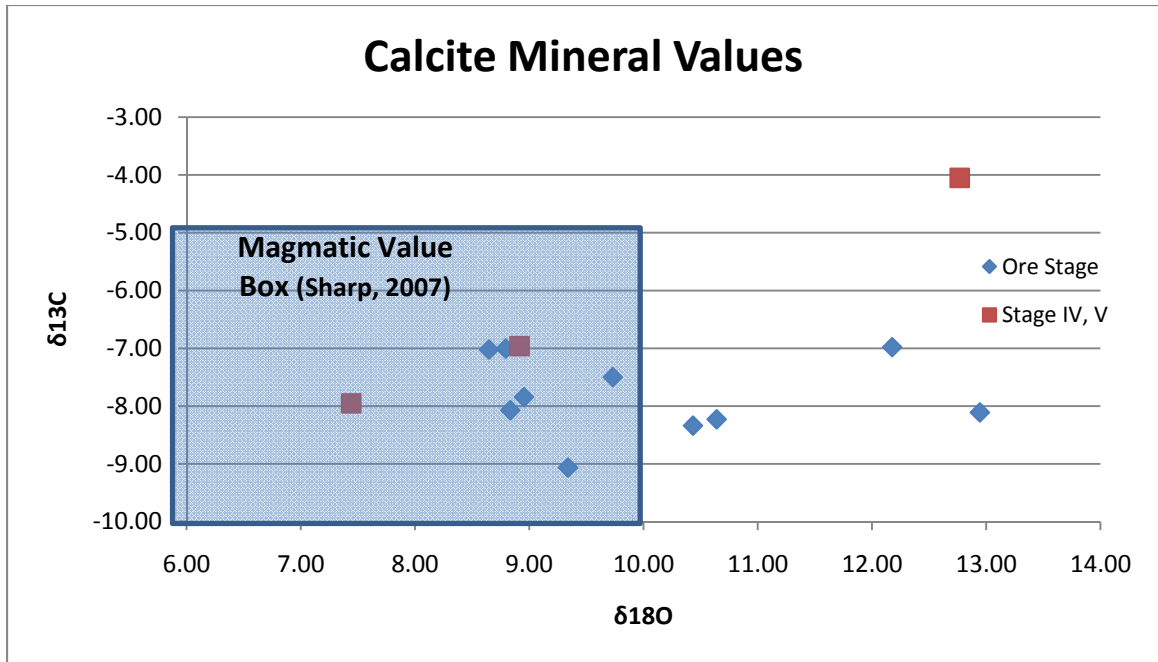


Figure 20. $\delta^{13}\text{C}$ versus $\delta^{18}\text{O}$ plot of analyzed calcite minerals. Shaded blue box represents typical magmatic carbonate values.

FLUID SOURCE DISCUSSION

The fluid inclusion and stable isotope information obtained through these analyses provides a framework to create potential models for how these ore deposits formed, both on a vein as well as district level.

The consistent $\delta^{34}\text{S}$ H_2S fluid values throughout the system suggests that the veins in Fresnillo Southwest all formed from a common source of sulfur. These values are also consistent with $\delta^{34}\text{S}$ sulfide values from the Manto and Chimney deposits of the Proaño Hill area analyzed by Partida et al. (1984). The Fresnillo Southwest area contains a median sulfide value of -5.3 ‰, which overlaps within error of the median value of -5.1 ‰ from sulfides within the Fortuna-Proaño area. This suggests these two zones of the district were formed from the same source of sulfur as the veins of Fresnillo Southwest.

The common source of sulfur can be most easily explained by a large-scale ore forming event that mineralized the different vein deposits throughout the district.

The $\delta^{34}\text{S}$ values analyzed from Fresnillo are however significantly different from the values reported from the majority of epithermal systems worldwide. The mineral and H_2S fluid $\delta^{34}\text{S}$ values from all mineral phases (pyrite, sphalerite, and galena) are lighter than what is reported in low or intermediate sulfidation epithermal systems (Christie and Robinson, 1992; Hassan-Nezhad and Moore, 2006; Klein et al., 2005; Simeone et al., 2005; So et al., 1995; Zoheir et al., 2008). A typical low sulfidation epithermal system contains $\delta^{34}\text{S}$ values of sulfide minerals around 0 to 4 ‰ (Figure 21). Deposits with this values, such as the Hauraki Goldfield of New Zealand, the Semna District of Egypt, and the deposits of the Kuril Island Arc are all interpreted as having a magmatic source of sulfur. Other deposits, such as the Panormos Bay deposits of Greece, and the Taxco District of Mexico, Fresnillo, have significantly lighter sulfide mineral values, and are interpreted as having sulfur sourced from the sedimentary rocks that host the deposits (Camprubí et al., 2006; Tombros et al., 2007). These are very similar to the Fresnillo district, which contains values from a range of -4 to -6‰, with a median of approximately -5 ‰. The incorporation of sedimentary sulfur has occurred in several deposits throughout the globe, and seems to be a reasonable explanation for the light values seen at Fresnillo.

These lighter values could either be a result of fractionation processes occurring during ore formation or a result of the geologic setting of the deposit itself. During disproportionation of SO_2 from a magma into aqueous sulfate and sulfide, fractionation causes the aqueous sulfide to have lighter values than either the coexisting sulfate or the

bulk sulfur composition of the original SO₂. Thus, the minerals that form from the light H₂S will also contain light δ³⁴S mineral values. This process is seen in high sulfidation epithermal systems such as Pascua Lama (Deyell et al., 2005) (Figure 21) and the Summitville mine (Rye, 1993). However, at Fresnillo, the oxidation state of the ore-forming fluids was too reducing to form significant sulfate species (Figure 17), and thus was dominated by H₂S-rich fluids. This fact makes this explanation relatively unlikely.

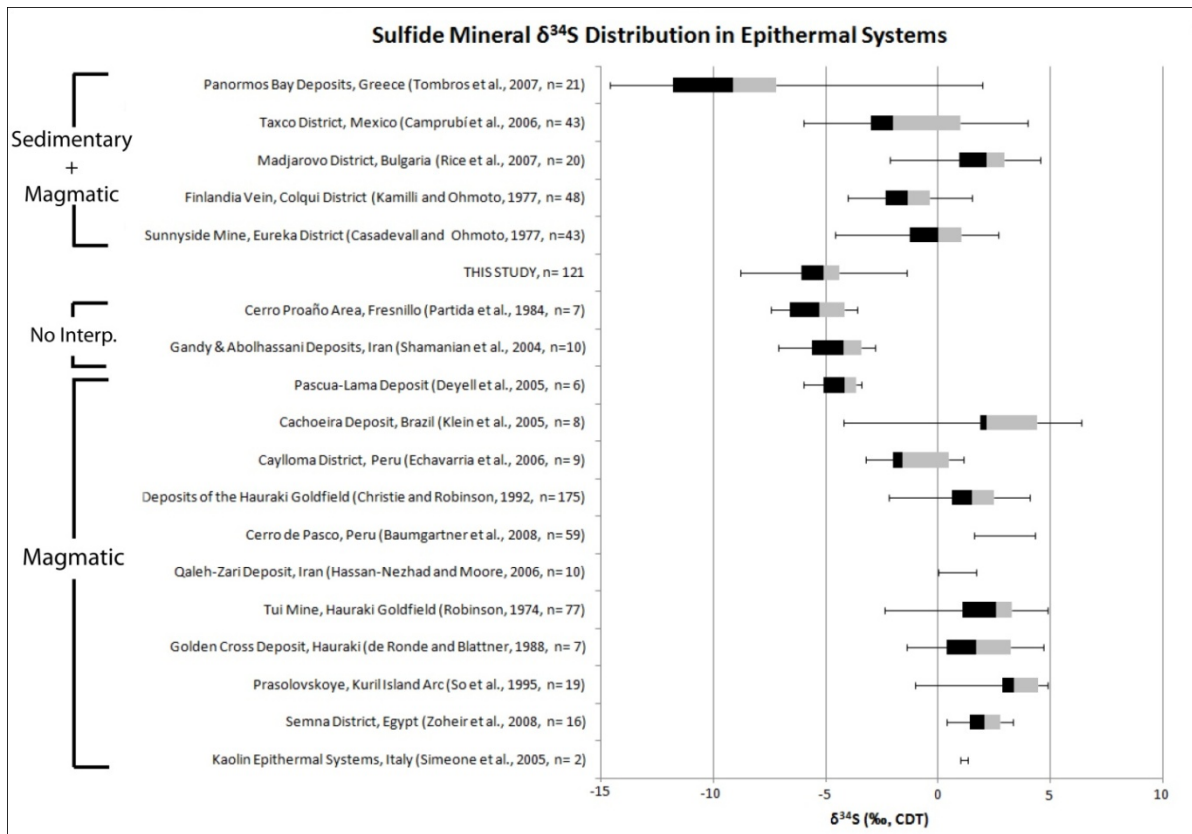


Figure 21. Mineral δ³⁴S values from epithermal systems from around the globe grouped by each author's interpretation of sulfur source. The intersection of the gray and black boxes represents the median sulfide mineral value, the edges of the boxes themselves represent the 25th and 75th percentiles, and the thin bars represent the total range of values of sulfides found at each deposit.

Alternatively the light values may be explained by the geologic setting in which the ores formed. The light δ³⁴S H₂S values might be the result of the incorporation of sedimentary sulfur into the ore forming fluids. The light values suggest a source of sulfur

different from magmatic sulfur, and could be at least partially derived from sediments within the Guerrero Terrane host unit. The extremely light $\delta^{34}\text{S}$ value of the sedimentary pyrite (-25.5 ‰) analyzed from the Guerrero Terrane supports this hypothesis. Given this hypothesis, the majority of the sulfur in Fresnillo would still be derived from a magmatic source, with $\delta^{34}\text{S}$ values near 0 ‰, with a lesser, but still significant, portion of total sulfur derived from the Guerrero host rock.

The incorporation of sedimentary sulfur into the ore forming fluids can be accomplished by two different processes (Figure 22). The first process would be the leaching of sedimentary pyrite from the host rocks by under-saturated meteoric waters, which were then mixed the magmatic fluids before metal deposition. However, the consistent, homogeneous values of sulfur throughout the western Fresnillo district suggest that if this process is responsible for introducing the light sedimentary sulfur, it must have been occurring at very deep levels within the system. A second explanation for the incorporation of sedimentary sulfur involves the assimilation of the Guerrero Terrane into the magmatic intrusion at depth. If a large portion of the sedimentary package was assimilated into the melt, the sulfur would homogenize within the intrusive unit, and make the fluids uniformly lighter. This model can best explain the consistent values across the district, as the mixing was occurring before the mineralizing event itself.

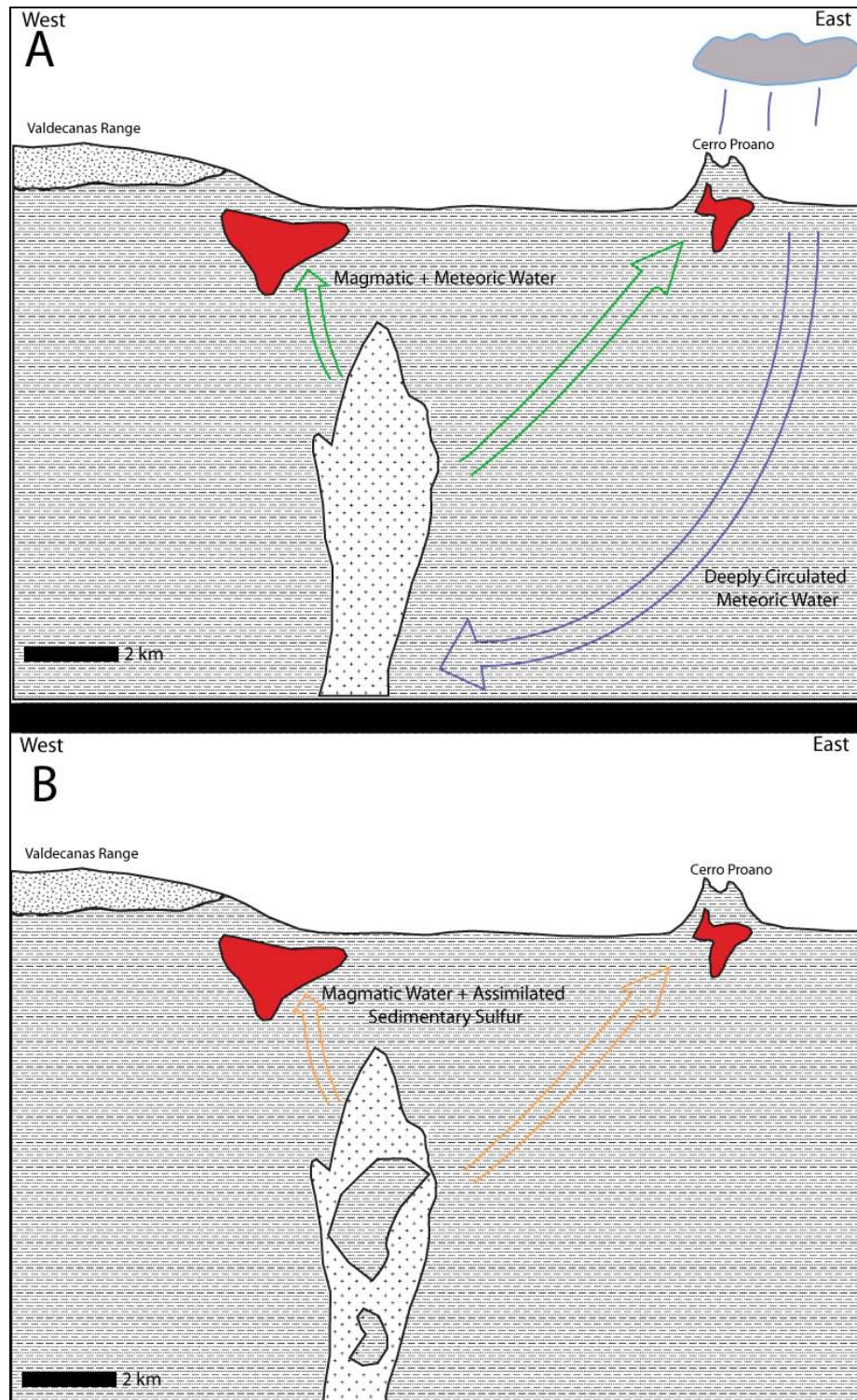


Figure 22. Cross Sections representing two sources of the ore forming fluid and the incorporation of sulfur into the system. Red portions represent mineralization. Figure A represents a model involving deeply circulating meteoric fluid and the leaching of reduced sulfur from the Guerrero hostrock. Figure B represents the assimilation of Guerrero Terrane into the intrusion itself.

The main distinction between these two processes involves the source of the ore-forming fluids. Thus, in order to understand the source of the metals within this deposit, it is crucial to identify which of these models accomplished the incorporation of the sulfur. In a leaching scenario, meteoric water would have to be incorporated into the ore-forming fluid, and it is possible that a portion of the metals within the deposit were leached from the sediments themselves. In the assimilation model, the fluid would be dominated by magmatic water, and metals would have been sourced solely from intrusive bodies. The $\delta^{18}\text{O}$ and δD values of fluids within the district can be interpreted as either magmatic or exchanged meteoric fluids, providing no additional information to help determine which of these mechanisms is more likely to have incorporated the sulfur. Like the $\delta^{18}\text{O}$ and δD of the ore forming fluids, fluid inclusion gas analysis data from the district provides no clear rationale to decide between the two scenarios. Published gas analysis data by (Benton, 1991) in the Santo Niño vein have been interpreted as reflecting a magmatic source of fluids. However, more recent gas analysis data from the Fresnillo Southwest district (Velador, 2010), suggests a meteoric source of fluids. Comparing this data is complicated by the fact that these two studies used different analytical techniques. Further study of the district will be necessary to be able to determine which of these mechanisms is responsible for the unique fluids present in the Fresnillo district.

This model of sedimentary sulfur contamination can be related to other deposits within the Guerrero Terrane. As observed by (Camprubí and Albinson, 2007), several sedimentary-hosted deposits within Mexico have light $\delta^{34}\text{S}$ mineral values. An example of this includes the Taxco district, located to the southeast of Fresnillo within the Morelos Formation (Guerrero Terrane), which includes lighter pyrite and sulfides than what is

common within other deposits (Camprubí et al., 2006). From these observations, it is apparent that a significant portion of the sulfides within the Southwest Fresnillo system, and potentially several other intermediate sulfidation systems within Mexico, was derived from sedimentary sulfur within the Guerrero Terrane itself.

CONCLUSIONS

The Southwest Fresnillo district contains high grade silver, gold, and base metal, epithermal vein-style mineralization. The Valdecañas vein, one of the largest of these recently discovered veins, seems to have formed over five distinct paragenetic stages, with *Stage III* being the main stage responsible for silver mineralization. Ore fluids that formed the veins were at temperatures between 160 to 320°C, with a modal temperature of 260°C. Salinities within the fluid were relatively low, ranging from 0.5 to 11 (average of 3.7) wt. % NaCl equivalent. The consistent and unusually light H₂S values of the ore forming fluids between the veins of the Fresnillo Southwest district indicate that the veins all formed from a common source of sulfur, and are probably related to the same ore-forming event. The consistent mineral values between Fresnillo Southwest and Cerro Proaño suggests that the ore forming event was district-wide, and could be responsible for the entirety of mineralization within Fresnillo. The light $\delta^{34}\text{S}$ values suggest the source of sulfur was not entirely magmatic, but incorporated significant amounts of light sedimentary sulfides from the Guerrero Terrane hostrocks. The incorporation of these sediments can be accomplished by two models—the leaching of sulfides out of the sediments by meteoric waters which were incorporated into the fluids, or the assimilation of Guerrero Terrane sediments into the magmatic body itself. The oxygen and hydrogen

isotope data of the ore-forming fluid can be interpreted as either highly exchanged, meteoric waters or magmatic waters. Gas analysis data from Velador (2010) suggests a meteoric source of fluids within Fresnillo Southwest; however, gas analysis data from (Benton, 1991) from Fresnillo SE can be interpreted as magmatic. There is a high probability that the source of the fluids in these systems is a mixture of both end members, and involves magmatic water exsolved from the intrusions as well as deeply circulated meteoric water. The mixing of these sources is consistent with the classification of Fresnillo as an intermediate sulfidation system, which has components of both high sulfidation (proximal to the intrusion with larger components of magmatic fluids), and low sulfidation (more distal with larger contributions of meteoric fluids) epithermal end members (Cooke and Simmons, 2000; Hedenquist et al., 2000).

Although the Fresnillo district is classified as an intermediate sulfidation epithermal system, the district appears to share many characteristics of low-sulfidation systems. The higher fluid salinities, high concentrations of base metals, and high silver to gold ratios are typical of intermediate sulfidation systems as described by (Camprubí and Albinson, 2007; Sillitoe and Hedenquist, 2003). However, the relatively low oxygen fugacities, lack of sulfate minerals, and presence of adularia within the system suggests low sulfidation style mineralization (Hedenquist et al., 2000; Sillitoe and Hedenquist, 2003). It is possible that the interaction with the Guerrero Terrane sediments, and the incorporation of components of the host rock into the ore forming fluids has produced this unique style of mineralization.

REFERENCES

- Baumgartner, R., Fontbote, L., and Vennemann, T., 2008, Mineral Zoning and Geochemistry of Epithermal Polymetallic Zn-Pb-Ag-Cu-Bi Mineralization at Cerro de Pasco, Peru: *Economic Geology*, v. 103, p. 493-537.
- Benton, L. D., 1991, Composition and source of the hydrothermal fluids of the Santo Niño vein, Fresnillo, Mexico, as determined from $^{87}\text{Sr}/^{86}\text{Sr}$, stable isotope, and gas analyses, New Mexico Tech.
- Bodnar, R. J., 1993, Revised equation and table for determining the freezing point depression of H₂O-NaCl solutions: *Geochim. Cosmochim. Acta*, v. 57, p. 683-684.
- Borthwick, J., and Harmon, R. S., 1982, A note regarding CIF₃ as an alternative to BrF₅ for oxygen isotope analysis: *Geochim. Cosmochim. Acta*, v. 46, p. 1665-1668.
- Buchanan, L. J., 1981, Precious metal deposits associated with volcanic environments in the southwest, *in* Dickinson, W. R., and Payne, W. D., eds., *Relations of Tectonics to Ore Deposits in the Southern Cordillera, XVI: Tucson, Arizona Geological Society Digest*, p. 237-262.
- Camprubí, A., and Albinson, T., 2007, Epithermal Deposits in Mexico--Update of current knowledge, and an empirical reclassification, *in* Alaniz-Alvarez, S. A., and Nieto-Samaniego, A. F., eds., *Geology of Mexico: Celebrating the Centenary of the Geological Society of Mexico: Geological Society of America Special Paper 422*, The Geological Society of America, p. 377-415.
- Camprubí, A., González-Partida, E., and Torres-Tafolla, E., 2006, Fluid inclusion and stable isotope study of the Cobre-Babilonia polymetallic epithermal vein system, Taxco district, Guerrero, Mexico: *Journal of Geochemical Exploration*, v. 89, p. 33-38.
- Casadevall, T., and Ohmoto, H., 1977, Sunnyside Mine, Eureka mining district, San Juan County, Colorado; geochemistry of gold and base metal ore deposition in a volcanic environment: *Economic Geology*, v. 72, p. 1285-1320.
- Christie, A. B., and Robinson, B. W., 1992, Regional sulphur isotope studies of epithermal Au-Ag-Pb-Zn-Cu deposits in the Hauraki Goldfield, South Auckland: *New Zealand Journal of Geology and Geophysics*, v. 35, p. 145-150.
- Cooke, D. R., and Simmons, S. F., 2000, Characteristics and Genesis of Epithermal Gold Deposits: *Reviews in Economic Geology*, v. 13, p. 221-244.
- De Cserna, Z., 1976, Geology of the Fresnillo Area, Zacatecas, Mexico: *Geological Society of America Bulletin*, v. 87, p. 1191-1199.

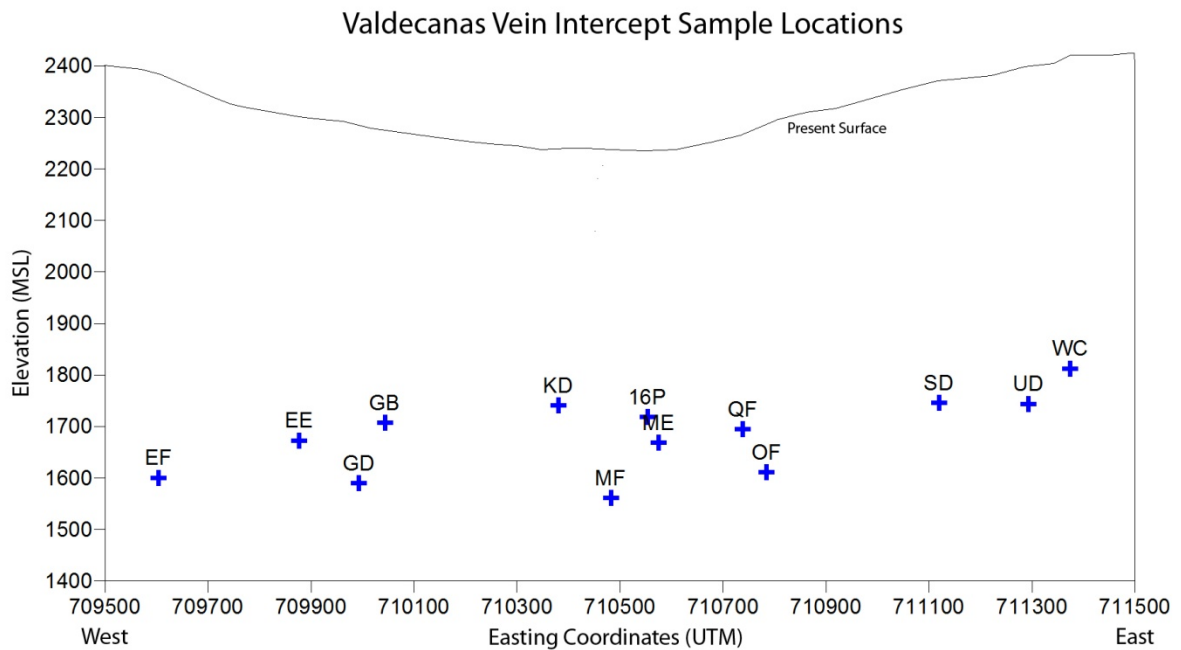
- de Ronde, C. E. J., and Blattner, P., 1988, Hydrothermal alteration, stable isotopes, and fluid inclusions of the Golden Cross epithermal gold-silver deposit, Waihi, New Zealand: *Economic Geology*, v. 83, p. 895-917.
- Deyell, C. L., Leonardson, R., Rye, R. O., Thompson, J. F. H., Bissig, T., and Cooke, D. R., 2005, Alunite in the Pascua-Lama High-Sulfidation Deposit: Constraints on Alteration and Ore Deposition Using Stable Isotope Geochemistry: *Economic Geology*, v. 100, p. 131-148.
- Dilley, L. M., 1993, Mineralogy and Fluid Inclusion Study of the San Mateo Vein, Fresnillo District, Zacatecas, Mexico: Socorro, New Mexico Institute of Mining and Technology.
- Echavarría, L., Nelson, E., Humphrey, J., Chavez, J., Escobedo, L., and Iriando, A., 2006, Geologic Evolution of the Caylloma Epithermal Vein District, Southern Peru: *Economic Geology*, v. 101, p. 843-863.
- Fresnillo PLC, 2010, Fresnillo Mine Annual Production Volumes, 2010.
- Gemmell, J. B., Simmons, S. F., and Zantop, H., 1988, The Santo Nino Silver-Lead-Zinc Vein, Fresnillo District, Zacatecas, Mexico: Part I. Structure, Vein Stratigraphy, and Mineralogy: *Economic Geology*, v. 83, p. 1597-1618.
- Hassan-Nezhad, A. A., and Moore, F., 2006, A stable isotope and fluid inclusion study of the Qaleh-Zari Cu-Au-Ag deposit, Khorasan Province, Iran: *Journal of Asian Earth Sciences*, v. 27, p. 805-818.
- Hedenquist, J. W., Arribas, A., and Gonzales-Urien, E., 2000, Exploration for epithermal gold deposits: *Reviews in Economic Geology*, v. 13, p. 245-277.
- Hedenquist, J. W., Claveria, R. J. R., and Villafuerte, G. P., 2001, Types of sulfide-rich epithermal deposits, and their affiliation to porphyry systems: Lepanto-Victoria-Far Southeast deposits, Philippines, as examples: ProExplo Congreso, Lima, Peru, April 24-28, 29, 2001.
- Kamilli, R. J., and Ohmoto, H., 1977, Paragenesis, zoning, fluid inclusion, and isotopic studies of the Finlandia Vein, Colqui District, central Peru: *Economic Geology*, v. 72, p. 950-982.
- Kim, S. T., and O'Neil, J. R., 1997, Equilibrium and nonequilibrium oxygen isotope effects in synthetic carbonates: *Geochim. Cosmochim. Acta*, v. 61, p. 3461-3475.
- Klein, E. L., Harris, C., Giret, A., Moura, C. A. V., and Angelica, R. S., 2005, Geology and stable isotope (O, H, C, S) constraints on the genesis of the Cachoeira gold deposit, Gurupi Belt, northern Brazil: *Chemical Geology*, v. 221, p. 188-206.

- Lang, B., Steinitz, G., Sawkins, F. J., and Simmons, S. F., 1988, K-Ar Age Studies in the Fresnillo Silver District, Zacatecas, Mexico: *Economic Geology*, v. 83, p. 1642-1646.
- Meheut, M., Lazzeri, M., Balan, E., and Mauri, F., 2007, Equilibrium isotopic fractionation in the kaolinite, quartz, water system: Prediction from first-principles density-functional theory: *Geochim. Cosmochim. Acta*, v. 71, p. 3170-3181.
- National Mining Association, 2008, Top World Silver Producers, National Mining Association.
- Ohmoto, H., and Rye, R. O., 1979, *Geochemistry of Hydrothermal Ore Deposits*: New York, Rinehart and Winston.
- Partida, E. G., Arnold, M., and Ayala, E. A., 1984, Análisis Metalogenético Preliminar del Distrito Minero de Fresnillo, Zacatecas Sobre la Base de 50 Medidas Isotópicas $\delta^{34}\text{S}$ ‰: *GEOMIMET*, v. 130, p. 27-34.
- Petersen, U., 1990, Ore Distribution, Zoning, and Exploration of Hydrothermal Ore Deposits: *Economic Geology*, v. 85, p. 424-435.
- Rice, C. M., McCoyd, R. J., Boyce, A. J., and Marchev, P., 2007, Stable isotope study of the mineralization and alteration in the Madjarovo Pb-Zn district, south-east Bulgaria: *Miner Deposita*, v. 42, p. 691-713.
- Robinson, B. W., 1974, The Origin of Mineralization at the Tui Mine, Te Aroha, New Zealand, in the Light of Stable Isotope Studies: *Economic Geology*, v. 69, p. 910-925.
- Roedder, E., 1984, *Fluid Inclusions*, Mineralogical Society of America, 644 p.
- Ruvalcaba-Ruiz, D. C., and Thompson, T. B., 1988, Ore Deposits at the Fresnillo Mine, Zacatecas, Mexico: *Economic Geology*, v. 83, p. 1583-1596.
- Rye, R. O., 1993, The Evolution of Magmatic Fluids in the Epithermal Environment: The Stable Isotope Perspective: *Economic Geology*, v. 88, p. 733-753.
- Shamanian, G. H., Hedenquist, J. W., Hattori, K. H., and Hassanzadeh, J., 2004, The Gandy and Abolhassani Epithermal Prospects in the Alborz Magmatic Arc, Semnan Province, Northern Iran: *Economic Geology*, v. 99, p. 691-712.
- Sharp, Z., 2007, *Principles of Stable Isotope Geochemistry: Upper Saddle River*, Pearson Prentice Hall.
- Sillitoe, R. H., and Hedenquist, J. W., 2003, Linkages between volcanotectonic settings, ore-fluid compositions, and epithermal precious-metal deposits: *Society of Economic Geologists, Special Publications Series*, v. 10, p. 315-343.

- Simeone, R., Dilles, J. H., Padalino, G., and Palomba, M., 2005, Mineralogical and Stable Isotope Studies of Kaolin Deposits: Shallow Epithermal Systems of Western Sardinia, Italy: *Economic Geology*, v. 100, p. 115-130.
- Simmons, S. F., Gemmell, J. B., and Sawkins, F. J., 1988, The Santo Nino Silver-Lead-Zinc Vein, Fresnillo District, Zacatecas, Mexico: Part II. Physical and Chemical Nature of Ore-Forming Solutions: *Economic Geology*, v. 83, p. 1619-1641.
- So, C.-S., Dunchenko, V. Y., Yun, S.-T., Park, M.-E., Choi, S.-G., and Shelton, K. L., 1995, Te- and Se-bearing epithermal Au-Ag mineralization, Prasolovskoye, Kunashir Island, Kuril island arc: *Economic Geology*, v. 90, p. 105-117.
- Tombros, S., Seymour, K. S., Williams-Jones, A. E., and Spry, P. G., 2007, The Genesis of Epithermal Au-Ag-Te Mineralization, Panormos Bay, Tinos Island, Cyclades, Greece: *Economic Geology*, v. 102, p. 1269-1294.
- Velador, J. M., 2010, Timing and origin of intermediate sulfidation epithermal veins and geochemical zoning in the Fresnillo District, Mexico: Constrained by $^{40}\text{Ar}/^{39}\text{Ar}$ geochronology, fluid inclusions, gas analysis, stable isotopes, and metal ratios, New Mexico Institute of Mining and Technology.
- Zoheir, B., Akawy, A., and Hassan, I., 2008, Role of fluid mixing and wallrock sulfidation in gold mineralization at the Semna mine area, central Eastern Desert of Egypt: Evidence from hydrothermal alteration, fluid inclusions and stable isotope data: *Ore Geology Reviews*, v. 34, p. 580-596.

APPENDIX I. VALDECAÑAS VEIN SAMPLE INFORMATION

Sample Location Longitudinal Section



Longitudinal Section of sampled vein intercepts of exploration drill core within the Valdecañas vein.

Valdecañas Vein Sample List

Table listing samples collected from the Valdecañas vein, including depth of core and a listing of minerals observed from initial hand specimen observations.

Sample Name	Depth (m, down core)	Minerals Present
VV-ME-01	684.7	qtz, chl, cc, dol, sl
VV-ME-02	686.9	qtz, sl, p, gn, cc, chl
VV-ME-03	687.4	sl, gn, py, vug qtz, qtz
VV-ME-04	688.3	qtz, sl, gn, py, hem. Chrt.
VV-ME-05	689.3	qtz, py, gn, sl
VV-ME-06	690.4	Mass. gn, sl, py, qtz, vug qtz, fl
VV-ME-07	691.4	Mass. gn, py, qtz

VV-ME-08	693.1	qtz, cc, +- py
VV-EE-01	772.8	qtz, chal qtz, py, sl, gn
VV-EE-02	774.3	py, qtz
VV-EE-03	775.3	vug qtz, cc, sl, chl, py
VV-EE-04	775.8	sl, py, gn, chl, qtz, hem. chrt
VV-EE-05	776.5	qtz, cc
VV-EE-06	776.8	
VV-EE-07	777.4	qtz, chal qtz, sl, gn, py
VV-EE-08	778	qtz, sl, gn, py
VV-EE-09	778.5	gn, sl, py
VV-EE-10	779	qtz, cc, sl
VV-EF-01	826	qtz, cc, py, sl, gn, chl
VV-EF-02	828.5	qtz, sl, py
VV-EF-03	830.1	qtz, slh qtz, chal qtz, sl, py, chl
VV-EF-04	830.6	qtz, sl, py, cpy
VV-EF-05	832.2	qtz, sl, gn, py, dol, vug qtz
VV-EF-06	837.8	qtz, gn, sl, py
VV-EF-07	833.4	qtz, sl, gn, py, barren cc
VV-EF-08	833.7	qtz, chl, py
VV-EF-09	834.5	qtz, cc, py, sl
VV-EF-10	835.9	qtz, py, Agss
VV-GB-01	726.2	qtz, chal qtz, py, hem chrt,
VV-GB-02	728.2	cc, py
VV-GB-03	731	qtz, sl, py
VV-GB-04	731.4	qtz, slh qtz, sl, py, sl
VV-GB-05	732	sl, gn, py
VV-QF-01	619.5	cc, chl
VV-QF-02	621.4	qtz, chal qtz, sl, py, gn
VV-QF-03	621.9	qtz, chl, sl, py, gn
VV-QF-04	622.8	qtz, sl, py, cc, mass. sl
VV-QF-05	623.2	qtz, chal qtz, sl, gn, py
VV-QF-06	623.4	qtz, sl, gn, py, chl
VV-QF-07	624.8	sl, py
VV-QF-08	625.5	qtz, py, chl, gn, sl
VV-QF-09	627.2	qtz, cc, py
VV-OF-01	789.1	qtz, cc, sl, py
VV-OF-02	789.9	qtz, sl, py
VV-OF-03	791.1	qtz, sl, py, gn, poss. cpy
VV-OF-04	791.4	qtz, sl, py, gn
VV-OF-05	793.6	qtz, sl, py, gn

VV-OF-06	794.9	Mass. sl, gn, py, qtz
VV-OF-07	795.3	vug qtz, sl, py, gn
VV-OF-08	796.6	qtz, chal qtz, sl
VV-OF-09	797.7	barren qtz, cc
VV-OF-10	798.1	sl, py, chrt, alteration minerals
VV-OF-11	799.3	mass gn, py, sl
VV-UD-01	744.6	qtz, sl, py
VV-UD-02	750.4	qtz, sl, gn, py
VV-UD-03	751.1	mass gn, py, sl, qtz, hem chrt
VV-UD-04	751.4	gn, py, sl, qtz, chal qtz
VV-UD-05	751.7	qtz, chal qtz, gn, py, sl, +- chl
VV-UD-06	753.1	qtz, sl, gn, py, chl, alteration minerals
VV-UD-07	753.5	qtz, sl, gn, py
VV-UD-08	754.1	mass gn, py, qtz, vug qtz
VV-UD-09	754.6	gn, sl, yellow-brown alteration
VV-WC-01	656	qtz, py
VV-WC-02	656.4	qtz vein, diss. py
VV-WC-03	661	qtz, py, sl, gn, poss. adularia or cc
VV-WC-04	661.4	py,gn, sl
VV-WC-05	662.6	qtz with poss. adula or cc
VV-WC-06	665.9	qtz, py
VV-KD-01	700.9	qtz, chal qtz, py
VV-KD-02	701.3	qtz, sl, py
VV-KD-03	703.1	qtz, cc, py, poss sl
VV-KD-04	704.3	py, gn, qtz, cc
VV-KD-05	704.9	qtz, sl, gn, py
VV-KD-06	705.8	qtz, sl, py, gn
VV-KD-07	706.7	qtz, chal qtz, py, sl
VV-KD-08	707.7	qtz, sl, py, cc
VV-KD-09	709.3	qtz, py, sl
VV-KD-10	710.5	qtz, sl, py
VV-SE-LU	656.3	Graywacke with lenses of ss in blk shale
VV-13P-2	688.1	med sl, coarse gn, fine py
VV-13P-3		fine py intgr w/ med gn. Qtz domin.
VV-16P-2	682.1	py w/intgr gn, sl
VV-16P-3	682.4	coarse sl, med py, late cc, pos. gn
VV-GD-1	791.4	py, sl intrgr w/ py
VV-GD-2	793.2	py, coase gn, poss. Sl
VV-GD-4	806.2	coarse gn, py, sl, poss cpy
VV-GD-5	806.8	coarse sl, coarse gn, fine py, cpy?

VV-GD-7	813.1	Mass. gn, med. py, poss. cpy
VV-GD-8	815.3	Mass. gn, py
VV-GD-9	816.3	fine py, sl?
VV-GD-10	818.4	sl w/intgr py, minor gn, qtz veins
VV-GD-11	818.8	massive gn, sl, py, cpy
VV-GD-12	821.1	fine py
VV-MF-1	813.8	qtz, py
VV-MF-3	816.55	Mass. gn, med sl, fine py
VV-MF-4	816.95	Mass. gn, py, cpy
VV-MF-5	818.95	py, coarse sl, gn
VV-MF-6	819.5	coarse gn, fine py, oxides
VV-MF-7	820.2	coarse py, coarse gn, sl
VV-SD-2	743.9	qtz, fine py surrounding med. sl
VV-SD-3	747.4	qtz with patches py, fine sl

Mineral abbreviations

gn=galena, sl=sphalerite, qtz=quartz, py=pyrite, cpy=chalcopyrite, chl=chlorite, adul=adularia, fl=fluorite, cc=calcite, chal=chalcedonic, hem= hematite, poss.= possible (not able to distinguish mineral with confidence)

APPENDIX II. PETROGRAPHIC DESCRIPTIONS BY DRILL HOLE AND SAMPLE NUMBER

EE Hole

EE-07

Transmitted Light Observations: Microcrystalline qtz along with medium qtz dominate left portion of the slide. Some greenish minerals (possibly chlorite) surround the opaque minerals (slhalerite), and are possibly alteration minerals. Calcite also present in slide, but only within the western half, immediately surrounding sulfides.

Medium to coarse grained qtz vein cuts pyrite within section. Coarse-medium qtz is followed and filled by microcrystalline qtz.

Reflected Light Observations: Galena with intergrown calcite is abundant on the western half of slide; almost no qtz present, only minor slhalerite. Sl seems to be dominantly confined to main vein structure, which is composed of py and sl+py, followed by quartz and later arsenopyrite

Pyrite is often surrounded by galena, suggesting it is older. However, there are several instances of cogenetic, intergrown pyrite within the slide as well.

EE-10

Transmitted Light Observations: Slide dominated by large, central qtz vein. Very coarse, and void of all sulfides. Can see very detailed paragenesis, beginning with coarse qtz layered with a medium qtz phase that has been filled by later calcite. This is followed by a thin py + qtz layer, a large coarse qtz stage, and another stage of calcite. Black oxides or clays are cut by coarse qtz and calcite vein. Clay present with qtz and calcite.

Reflected Light Observations: Slhalerite present throughout slide, and is intergrown with py and gn. Sl has cp disease. No visible arsenopyrite is present. Some py is overgrown by gn, suggesting an earlier stage of pyrite.

Paragenesis: coarse qtz → medium qtz → calcite → coarse qtz → calcite, sulfides (py → sl+gn+py)

EF Hole

EF-04

Transmitted Light Observations: Medium-coarse qtz dissected by microcrystalline qtz veins. Microcrystalline quartz has brecciated sulfides within it suggesting this phase is post-sulfides. Sulfides appear to be related to medium-qtz phase. Another, later medium stage is also present, and cuts microcrystalline veins. Minor calcite, (dirty, lots of opaques) is cementing sulfide minerals. Some clays associated with microcrystalline qtz as well.

Reflected Light Observations: Sl associated with py and asly, and contains cp and silver sulfide disease. Galena also present within sl. Two episodes of py exist within the slide, one surrounding sl and one being surrounded.

Paragenesis: medium-coarse qtz→sulfides→microcrystalline qtz→medium qtz→calcite
(sulfides: py→sl+gn+py+asly→py)

EF-08b

Transmitted Light Observations: Slide dominated by qtz and massive calcite, intergrown within each other. Central band of sulfides present. Seems to be two episodes of calcite deposition, one with qtz, including both coarse and microcrystalline qtz, and a later calcite and coarse qtz stage infilling and brecciating the section. Sulfides surrounded by calcite and patches of qtz, with minor chlorite.

Reflected Light Observations: Sl is present in bands, and includes cp and silver sulfide disease. Sl formed syngenetically with py, and arsenopyrite is present on the outer edges of sl. Galena seems to be cogenetic with sl, or slightly earlier. Minor cp with py also present away from main sl band.

Paragenesis: medium-coarse qtz→microcrystalline→calcite→calcite+ coarse qtz
(sulfides: sl+gn+py →py+asly+cp)

GB Hole

GB-02

Transmitted Light Observations: Large vein within section composed of calcite lining a center of middle-coarse quartz. Calcite seems to be syngenetic or possibly deposited after the sulfide minerals.

Reflected Light Observations: Pyrite present surrounding gn. Sl contains intergrown py, suggesting the two phases are coeval.

Paragenesis: cc+sulfides → medium quartz

GD Hole

GD-04

Transmitted Light Observations: Coarse calcite and quartz are present throughout the sample. These two minerals surround sulfides, so these minerals appear to be post-sulfide deposition.

Reflected Light Observations: Chalcopyrite is present in significant amounts within this slide, usually surrounding pyrite, slhalerite, and galena, and appears to be the last sulfide to form. Slhalerite and galena occur first, followed by pyrite. No Asly present within the sample.

Paragenesis: sl+gn → py→cp (qtz→microcrystalline qtz→calcite)

GD-10

Transmitted Light Observations: Some chalcedonic (botrioidal) bands of quartz are present within medium grained quartz. Calcite present within the void slaces of pyrite and slhalerite, and appears to have in-filled the grains. Calcite is also found occasionally within quartz grains, also appearing to have in-filled the grains.

Reflected Light Observations: Pyrite and Sphalerite are the dominant sulfides, with abundant, but less common, galena. Galena is surrounded by pyrite in most cases. Large sphalerite patches sometimes contain galena in the interior, suggesting that galena was slightly earlier in this section. Sulfides are cut by fine-medium quartz, and also by calcite veins. Arsenopyrite is not present within this sample.

Paragenesis: $qtz \rightarrow gn+sl \rightarrow \text{micro } qtz \rightarrow \text{calcite}$

KD Hole

KD-05

Transmitted Light Observations: Slide dominated by calcite, with small patches of quartz. Quartz usually lines sulfide veins, appears to be syngenetic with or slightly after sulfide deposition. Large sulfide chunks (brecciated) are surrounded by calcite, which appears to be later.

Reflected Light Observations: Sulfides include sphalerite with galena chunks within the sphalerite. Sphalerite also has significant copper and silver sulfide disease. Sphalerite is lined by a lining of pyrite. Arsenopyrite is also present within quartz and calcite.

Paragenesis: $\text{sulfides} \rightarrow \text{quartz} \rightarrow \text{calcite}$ (sulfides: $py \rightarrow py+sl+gn \rightarrow py+asly$)

KD-08

Transmitted Light Observations: Very complicated, sinuous vein system with primarily calcite and quartz. Vein is divided into several bands of quartz, sulfides, and calcite. Core is quartz, followed by sphalerite band, and then calcite. From the textures, it appears that sulfides formed first, followed by fine quartz, then larger, medium quartz, and finally calcite. Some pieces of pyrite present within the calcite.

Reflected Light Observations: Sulfides include sphalerite, with copper and minor silver sulfide disease. Arsenopyrite and pyrite are also common, present in almost equal amounts. Appears that pyrite was present throughout formation, arsenopyrite present as a later stage.

Paragenesis: $\text{sulfides} \rightarrow \text{quartz} \rightarrow \text{sulfides} \rightarrow \text{calcite} \rightarrow \text{sulfides} \rightarrow \text{calcite}$ (sulfides: $py+sl \rightarrow py+asly$)

ME Hole

ME-02

Transmitted Light Observations: Four different stages of quartz, including an early coarse quartz, followed by microcrystalline quartz, medium quartz, and possibly a second stage of coarse quartz. Calcite appears to be the last gangue mineral to form. Microcrystalline quartz is directly touching sulfides, and appears to have formed immediately after.

Reflected Light Observations: Large bands of sphalerite with copper disease and possibly silver sulfides evolved within sphalerite. Lined by pyrite, large patches of galena appear to cut (or potentially just cogenetic with) sphalerite. Some pyrite cutting sphalerite too.

Paragenesis: $\text{coarse } qtz \rightarrow \text{sulfides} (py+sl+gn \rightarrow py) \rightarrow \text{micro } qtz \rightarrow \text{coarse } qtz \rightarrow \text{calcite}$

ME-05

Transmitted Light Observations: Quartz and calcite (both very coarse grained) cut pyrite. Fine calcite has cut into massive pyrite.

Reflected Light Observations: Veins of pyrite cut heavily pitted sphalerite. Sphalerite cuts large, euhedral patches of pyrite. Galena is present, but almost appears to be replaced by sphalerite or is significantly oxidized or altered. The galena is not fresh, and is most likely coeval with sphalerite.

Paragenesis: Pyrite→ sphalerite+gn→ quartz+cc

MF Hole

MF-04

Transmitted Light Observations: Qtz veins cut sl and galena and are medium to coarse grained.

Reflected Light Observations: Some pyrite within these veins and bands of quartz. Galena is found isolated within pyrite. Sphalerite and galena are abundant and grown together in many cases. Sphalerite has cp disease. Some chlorite or clay alteration present. Also see very fuzzy pyrite in SW portion of the slide—possibly altered

MF-05

Transmitted Light Observations: Medium to fine qtz veins cut sphalerite and galena, suggesting that the main vein in the section is post-sulfides, cutting both sl, gn, and pyrite. Microcrystalline qtz seems to be syngenetic with the sulfides.

Reflected Light Observations: Pyrite lines the edges of these veins (earlier than the later quartz). Pieces of pyrite are also found within the vein, brecciated by quartz. Sl+gn intergrown and surrounded by py. No asly was found in the section. Sphalerite has exsolved phases, but it is difficult to determine what minerals are present due to the small bleb size.

Paragenesis: sulfides+microcrystalline qtz → larger qtz

OF Hole

OF-1

Transmitted Light Observations: Coarse qtz within the section is cut by thin veinlets (100-200um) of fine qtz. Calcite present associated with fine qtz in wider portions of veinlets, and appears to be a later phase of mineralization

Reflected Light Observations: Sulfides are present in minor quantities compared to other sections, and include sl with cp disease and either silver sulfides/sulfosalts or exsolved gn. Some disseminated py also present, but relatively minor.

Paragenesis: coarse qtz→fine qtz→ calcite

QF Hole

QF-2

Transmitted Light Observations: Microcrystalline qtz cuts medium quartz. Calcite fills vugs within microcrystalline phase, suggesting calcite formed late in this stage of mineralization. Another later medium qtz phase occurs after microcrystalline qtz, which appears to also be infilled by calcite. “Dirty,” gray calcite appears to be the 1st stage, followed by a “cleaner” calcite stage. There is no other major differences between the calcite, however, and the different appearances could be related to differences in slide thickness.

Reflected Light Observations: Euhedral pyrite is surrounded by gn in portions of the section, suggesting a euhedral, early stage of pyrite. Gn is surrounded by sl, and vice versa, suggesting sl and gn are intergrown and cogenetic. Another morphology of pyrite, with subhedral grains, surrounds sl+gn, and formed later. No Asly present within sample.

Paragenesis: medium-coarse qtz → sl+gn → microcrystalline qtz → “dirty” calcite → medium qtz → “clean” calcite

QF-5

Transmitted Light Observations: Medium grained (~20-30um) quartz is found in contact with sulfides and seems to be earliest quartz. This is surrounded by a fine (<10um) quartz matrix, which seems to be later and surrounds brecciated sulfides. Calcite is being rimmed by very coarse quartz in one section of slide (no major sulfides) A vein on the eastern side of slide contains coarse qtz and patches of calcite, and seems to cut other quartz and sulfides. This suggests the calcite and coarse quartz occurred late in the paragenesis.

Reflected Light Observations: Galena and slhalerite are typically intergrown, making it difficult to tell their order of formation (assuming these minerals to be cogenetic). Slhalerite has cp disease. Pyrite seems to have overgrown both slhalerite and galena, but is also included within some slhalerite, suggesting that py was forming over a significant portion of the mineralization within the section.

Paragenesis: medium-coarse qtz → sl+gn → microcrystalline qtz → calcite → medium qtz

QF-7

Transmitted Light Observations: Eastern portion of slide is calcite-rich with massive, coarse grained quartz. Veins of these coarse minerals have overtaken many medium and smaller quartz veins. Microcrystalline qtz seems earliest, followed by coarse qtz, and then massive calcite

Reflected Light Observations: Sulfides are associated with medium to coarse (overgrown?) quartz. Slhalerite and galena seem to be cogenetic or massively intergrown. Slhalerite has cp disease within many grains, pyrite is rimming and overgrowing sl+gn, but some py appears within sl, so could be two separate stages

Paragenesis: microcrystalline qtz → medium qtz → sl+gn → calcite

WC Hole

WC-01

Transmitted Light Observations: Sulfides cut by fine-medium qtz veins, fine qtz and clay veins cut coarser qtz and sulfides. Adularia is present within large qtz grains, altering slightly to clay. Brecciated coarse qtz found within finer-medium qtz.

Reflected Light Observations: Sulfides include py, cp, and minor gn. Galena is first in the paragenesis, and is broken up by later py. The pyrite was then broken up by even later cp.

Paragenesis: Coarse qtz→fine-medium qtz→microcrystalline (sulfides: gn→py→cp)

Sedimentary Sections

SE-Guerrero

Sample taken from depth of within SE drill core, approximately 200 meters above vein intercept. Consists of greywacke sandstone lenses within black shales. Some small veins cut rock, could be calcite, or deposited within original sediment.

BNO-R7 Section 1

Very large nodule of pyrite—almost resembles a sedimentary nodule. No large veins nearby or within section. Some very small cc veinlets cut host Guerrero rock, but no sulfides visible within them.

Pyrite grains are large and euhedral, show no framboidal textures. Nothing definitive to indicate sedimentary origin. Dr. Mozley believes he sees shear structures within some pyrite grains, could be a result of tectonic forces. Is not definitive, however.

BNO-R7 Section 2

Very fine mudrock with sparse, disseminated pyrite. Pyrite grains are ~25um in size, very fine. No signs of sedimentary or hydrothermal origin.

APPENDIX III. FLUID INCLUSION DATA

Sample	Mineral Type	Stage	Size (µm)	Fill (%L)	Th (°C)	Tm (°C)	Salinity (wt. % NaCl eq.)
STAGE V INCLUSIONS							
EE-03	Coarse Calcite	V	15	85	296.5	-1.6	2.7
EE-03	Coarse Calcite	V	4	95	288.5	-2	3.4
EE-03	Coarse Calcite	V	6	90	267.5	-1.6	2.7
GD-04	Coarse Calcite	V	7	85	216.5	-3	5.0
GD-04	Coarse Calcite	V	8	90	216.5	-3.1	5.1
GD-04	Coarse Calcite	V	8	90	217.5	-3.1	5.1
GD-04	Coarse Calcite	V	10	95	220.5	-2.3	3.9
GD-04	Coarse Calcite	V	8	90	212.5	-3	5.0
GD-04	Coarse Calcite	V	10	90	220.5	-3	5.0
GD-04	Coarse Calcite	V	15	90	217.5	-1.9	3.2
EE-03	Coarse Qtz	V	8	90	258.5	-1	1.7
EE-03	Coarse Qtz	V	18	90	260.5	-0.5	0.9
EE-03	Coarse Qtz	V	12	80	298.5	-0.4	0.7
GD-04	Coarse Qtz	V	20	95	221.5	-2.6	4.3
GD-04	Coarse Qtz	V	20	90	217.5	-2.8	4.6
GD-04	Coarse Qtz	V	10	95	193.5	-2.6	4.3
GD-04	Coarse Qtz	V	10	95	204.5	-2.5	4.2
GD-04	Coarse Qtz	V	15	85	214.5	-2.4	4.0
GD-04	Coarse Qtz	V	10	90	238.5	-2.7	4.5
GD-04	Coarse Qtz	V	10	90	210.5	-2.7	4.5
GD-04	Coarse Qtz	V	4	90	247.5	-2.8	4.6
GD-04	Coarse Qtz	V	15	95	248.5	-2.7	4.5
GD-04	Coarse Qtz	V	10	90	233.5	-2.8	4.6
GD-04	Coarse Qtz	V	10	85	225.5	-2.3	3.9
GD-04	Coarse Qtz	V	8	90	220.5	-2.7	4.5
ME-08	Coarse Qtz	V	15	90	189.5	-1.2	2.1
ME-08	Coarse Qtz	V	6	85	255.5	-1.1	1.9
ME-08	Coarse Qtz	V	8	90	254.5	-2	3.4
ME-08	Coarse Qtz	V	8	95	204.5	-0.7	1.2
ME-08	Coarse Qtz	V	20	90	275.5	-2.7	4.5
ME-08	Coarse Qtz	V	8	95	309.5	-3.4	5.6
ME-08	Coarse Qtz	V	20	90	217.5	-1.7	2.9
ME-08	Coarse Qtz	V	4	95	216.5	-2.6	4.3
ME-08	Coarse Qtz	V	20	90	216.5	-1.5	2.6

ME-08	Coarse Qtz	V	6	90	209.5	-1.6	2.7
ME-08	Coarse Qtz	V	8	90	239.5	-1.4	2.4
QF-7	Coarse Quartz	V	8	95	261.5	-0.7	1.2
QF-7	Coarse Quartz	V	8	90	252.5	-0.7	1.2
QF-7	Coarse Quartz	V	8	80	258.5	-0.4	0.7
QF-7	Coarse Quartz	V	5	90	254.5	-0.7	1.2
QF-7	Coarse Quartz	V	6	85	248.5	-1.2	2.1
QF-7	Coarse Quartz	V	6	90	248.5	-0.6	1.1
QF-7	Coarse Quartz	V	6	90	256.5	-2.2	3.7
QF-7	Coarse Quartz	V	10	90	248.5	-2	3.4
QF-7	Coarse Quartz	V	10	90	254.5	-2.2	3.7
QF-7	Coarse Quartz	V	5	95	248.5	-1.7	2.9
QF-7	Coarse Quartz	V	6	90	260.5	-1.4	2.4
QF-7	Coarse Quartz	V	6	85	302.5	-0.5	0.9
QF-7	Coarse Quartz	V	6	85	288.5	-0.6	1.1
QF-7	Coarse Quartz	V	5	80	295.5	-0.5	0.9
QF-7	Coarse Quartz	V	5	85	290.5	-0.6	1.1
QF-7	Coarse Quartz	V	18	90	246.5	-5.3	8.3
QF-7	Coarse Quartz	V	10	90	241.5	-5.2	8.1
QF-7	Coarse Quartz	V	12	90	253.5	-3.8	6.2
QF-7	Coarse Quartz	V	6	90	265.5	-2.4	4.0
QF-7	Coarse Quartz	V	5	95	263.5	-2.6	4.3
EE-03	Qtz Crystal Center	V	7	95	201.5	-1.2	2.1
EE-03	Qtz Crystal Center	V	8	95	210.5	-1.4	2.4
EE-03	Qtz Crystal Center	V	5	90	224.5	-1.2	2.1
EE-03	Qtz Crystal Inner	V	18	95	310.5	-1.3	2.2
EE-03	Qtz Crystal Inner	V	10	85	275.5	-1.2	2.1
EE-03	Qtz Crystal Inner	V	6	90	268.5	-1.3	2.2
EE-03	Qtz Crystal Inner	V	10	90	261.5	-1.1	1.9
EE-03	Qtz Crystal Outer	V	10	80	262.5	-1.9	3.2
EE-03	Qtz Crystal Outer	V	88	60	249.5	-1.9	3.2
ORE STAGE INCLUSIONS							
EE-06	Coarse Opn Slc Qtz	III	9	90	215.5	-1.7	2.9
EE-06	Coarse Opn Slc Qtz	III	8	95	197.5	-1.8	3.1
EE-06	Coarse Opn Slc Qtz	III	10	90	256.5	-7.3	10.9
EE-06	Coarse Opn Slc Qtz	III	7	90	284.5	-7.3	10.9
EE-06	Coarse Opn Slc Qtz	III	5	95	269.5	-7.1	10.6
EE-06	Coarse Qtz	III	12	98	184.5	-2.1	3.5
EE-06	Coarse Qtz	III	8	95	238.5	-1.5	2.6
EE-06	Coarse Qtz	III	13	95	190.5	-5.5	8.5

EE-06	Coarse Qtz	III	15	90	215.5	-1.7	2.9
EE-06	Coarse Qtz	III	8	95	228.5	-1.4	2.4
EE-06	Coarse Qtz	III	5	90	230.5	-1.8	3.1
EE-06	Coarse Qtz Window	III	6	95	188.5	-2.7	4.5
EE-06	Coarse Qtz Window	III	15	95	213.5	-2	3.4
EE-06	Min Qtz	III	20	98	212.5	-5.5	8.5
EE-06	Min Qtz	III	4	95	170.5	-1.3	2.2
EE-06	Min Qtz	III	5	95	254.5	-2.7	4.5
EE-06	Min Qtz	III	12	90	243.5	-5.5	8.5
EE-06	Min Qtz	III	15	90	258.5	-7.5	11.1
EE-06	Min Qtz	III	8	95	218.5	-2.6	4.3
EE-10	Coarse Calcite Bd. B	III	8	95	176.5	-0.5	0.9
EE-10	Coarse Calcite Bd. B	III	10	95	169.5	-0.6	1.1
EE-10	Coarse Calcite Bd. B	III	8	90	245.5	-0.6	1.1
EE-10	Coarse Calcite Bd. B	III	18	95	168.5	-0.5	0.9
EE-10	Coarse Qtz Band A	III	8	85	262.5	-1.2	2.1
EE-10	Coarse Qtz Band A	III	12	90	200.5	-0.2	0.4
EE-10	Coarse Qtz Band A	III	4	95	174.5	-0.2	0.4
EE-10	Coarse Qtz Band A	III	8	90	208.5	-0.3	0.5
EE-10	Coarse Qtz Band A	III	4	95	177.5	-0.7	1.2
EE-10	Coarse Qtz Band A	III	6	95	183.5	-0.8	1.4
EE-10	Coarse Qtz Band A	III	4	90	244.5	-1.7	2.9
EE-10	Coarse Qtz Band A	III	5	90	257.5	-0.8	1.4
EE-10	Coarse Qtz Band B	III	18	95	166.5	-0.2	0.4
EE-10	Coarse Qtz Band B	III	20	90	171.5	-0.2	0.4
EE-10	Coarse Qtz Band B	III	15	90	163.5	-0.2	0.4
EE-10	Coarse Qtz Band B	III	8	90	240.5	-0.6	1.1
EE-10	Coarse Qtz Band B	III	8	95	153.5	-1.3	2.2
EE-10	Coarse Qtz Band B	III	8	95	240.5	-0.6	1.1
EE-10	Coarse Qtz Band B	III	8	95	234.5	-0.4	0.7
EE-10	Coase Qtz, Bd. B	III	5	95	200.5	-7.6	11.2
EE-10	Coase Qtz, Bd. B	III	6	95	250.5	-7.6	11.2
EE-10	Coase Qtz, Bd. B	III	8	90	202.5	-6.6	10.0
EF-04	Coarse Opn Slc Qtz	III	15	95	171.5	-0.1	0.2
EF-04	Coarse Opn Slc Qtz	III	8	95	209.5	-0.2	0.4
EF-04	Coarse Opn Slc Qtz	III	6	95	170.5	-0.2	0.4
EF-04	Coarse Opn Slc Qtz	III	10	95	200.5	0	0.0
EF-04	Coarse Opn Slc Qtz	III	15	82	250.5	-0.4	0.7
EF-04	Coarse Opn Slc Qtz	III	8	95	254.5	-0.4	0.7
EF-04	Coarse Opn Slc Qtz	III	10	95	253.5	-0.5	0.9

EF-04	Coarse Opn Slc Qtz	III	8	90	258.5	-0.7	1.2
EF-04	Coarse Opn Slc Qtz	III	5	95	253.5	-0.8	1.4
EF-04	Coarse Qtz	III	13	95	248.5	-3.3	5.4
EF-04	Coarse Qtz	III	15	90	243.5	-3.8	6.2
EF-04	Coarse Qtz	III	8	95	257.5	-1.1	1.9
EF-04	Coarse Qtz	III	8	90	280.5	-0.3	0.5
EF-04	Coarse Qtz	III	12	90	260.5	-0.4	0.7
EF-04	Coarse Qtz	III	6	95	205.5	-0.3	0.5
EF-04	Coarse Qtz	III	8	90	289.5	-1.1	1.9
EF-04	Coarse Qtz	III	5	95	286.5	-1.1	1.9
EF-04	Coarse Qtz	III	8	95	259.5	-0.8	1.4
EF-04	Coarse Qtz	III	8	90	252.5	-0.8	1.4
EF-04	Coarse Qtz	III	6	95	224.5	-0.8	1.4
EF-04	Coarse Qtz	III	8	85	305.5	-0.9	1.6
EF-04	Coarse Qtz	III	2	95	238.5	-1.5	2.6
EF-08a	Coarse Calcite	III	4	95	199.5	-0.7	1.2
EF-08a	Coarse Calcite	III	5	85	260.5	-0.6	1.1
EF-08a	Coarse Calcite	III	8	90	259.5	-1.3	2.2
EF-08a	Coarse Qtz	III	8	95	263.5	-0.5	0.9
EF-08a	Coarse Qtz	III	8	90	261.5	-0.4	0.7
EF-08a	Coarse Qtz	III	10	95	286.5	-0.5	0.9
EF-08a	Coarse Qtz	III	8	95	276.5	-0.9	1.6
EF-08a	Coarse Qtz	III	4	90	256.5	-1.2	2.1
EF-08a	Coarse Qtz	III	7	95	249.5	-1.4	2.4
EF-08a	Coarse Qtz	III	10	90	279.5	-1.7	2.9
EF-08a	Coarse Qtz	III	8	90	246.5	-1.7	2.9
EF-08a	Coarse Qtz	III	8	95	251.5	-2.1	3.5
EF-08a	Coarse Qtz	III	8	85	271.5	-1.4	2.4
EF-08a	Coarse Qtz	III	6	95	239.5	-3.2	5.3
EF-08a	Coarse Qtz	III	6	95	272.5	-3.3	5.4
EF-08a	Coarse Qtz	III	8	95	279.5	-0.6	1.1
EF-08a	Coarse Qtz	III	6	90	267.5	-0.5	0.9
EF-08a	Coarse Qtz	III	4	95	257.5	-0.4	0.7
EF-08a	Coarse Qtz	III	8	90	250.5	-1.3	2.2
EF-08a	Coarse Qtz	III	6	95	268.5	-5.9	9.1
EF-08a	Coarse Qtz	III	8	90	237.5	-1.7	2.9
GB-02	Coarse Calcite	III	10	90	241.5	-0.4	0.7
GB-02	Coarse Calcite	III	10	90	288.5	-0.3	0.5
GB-02	Coarse Calcite	III	18	90	265.5	-0.9	1.6
GB-02	Coarse Calcite	III	7	95	223.5	-0.5	0.9

GB-02	Coarse Calcite	III	20	95	180.5		
GB-02	Coarse Calcite	III	8	95	158.5		
GB-02	Coarse Calcite	III	12	95	261.5	-2.2	3.7
GB-02	Coarse Calcite	III	6	95	189.5		
GB-02	Coarse Calcite	III	6	95	246.5	-2.6	4.3
GB-02	Coarse Calcite	III	8	95	237.5	-2.8	4.6
GB-02	Coarse Calcite	III	12	75	259.5	-2.4	4.0
GB-02	Coarse Qtz	III	10	95	210.5	-6.6	10.0
GB-02	Coarse Qtz	III	8	95	221.5	-6.8	10.2
GB-02	Coarse Qtz	III	12	95	150.5	-6.3	9.6
GB-02	Coarse Qtz	III	15	98	180.5	-6	9.2
GB-02	Coarse Qtz	III	6	95	235.5	-1.4	2.4
GB-02	Coarse Qtz	III	5	95	222.5	-1.3	2.2
GB-02	Coarse Qtz	III	6	90	212.5	-1.4	2.4
GB-02	Coarse Qtz	III	7	95	249.5	-0.9	1.6
GB-02	Coarse Qtz	III	4	95	248.5	-1.4	2.4
GB-02	Coarse Qtz	III	8	95	256.5	-1.1	1.9
GB-02	Coarse Qtz	III	7	95	247.5	-1	1.7
GD-02	Min Qtz	III	13	90	281.5	-5.5	8.5
GD-02	Min Qtz	III	8	95	299.5	-5.3	8.3
GD-02	Min Qtz	III	6	85	308.5	-4.8	7.6
GD-02	Min Qtz	III	8	95	263.5	-5.1	8.0
GD-02	Min Qtz	III	15	88	280.5	-4.9	7.7
GD-02	Min Qtz	III	7	90	293.5	-3.3	5.4
GD-02	Min Qtz	III	12	95	291.5	-3.6	5.9
GD-02	Min Qtz	III	5	85	273.5	-6.6	10.0
GD-02	Min Qtz	III	8	80	297.5	-3.4	5.6
GD-02	Min Qtz	III	10	85	284.5	-6.4	9.7
GD-02	Min Qtz	III	8	75	276.5	-3.3	5.4
GD-02	Min Qtz	III	20	95	202.5	-5.5	8.5
GD-02	Min Qtz	III	10	90	222.5	-5.8	8.9
GD-02	Min Qtz	III	7	95	221.5	-6.4	9.7
GD-02	Min Qtz	III	4	90	219.5	-6.3	9.6
GD-02	Min Qtz	III	4	90	222.5	-6.2	9.5
GD-02	Min Qtz	III	6	90	225.5	-3.3	5.4
GD-05	Min Qtz	III	7	90	221.5	-4.2	6.7
KD-05	Coarse Calcite	III	8	85	263.5	-1.4	2.4
KD-05	Coarse Calcite	III	6	85	263.5	-1.7	2.9
KD-05	Coarse Calcite	III	7	90	249.5	-2.7	4.5
KD-05	Coarse Calcite	III	8	95	251.5	-4.4	7.0

KD-05	Coarse Calcite	III	9	85	291.5	-1.4	2.4
KD-05	Coarse Calcite	III	12	95	258.5	-1.4	2.4
KD-05	Coarse Calcite	III	8	90	263.5	-1.3	2.2
KD-05	Coarse Calcite	III	15	95	262.5	-1.3	2.2
KD-05	Coarse Calcite	III	10	90	224.5	-0.5	0.9
KD-05	Coarse Calcite	III	8	90	239.5	-3.7	6.0
KD-05	Coarse Calcite	III	6	95	244.5	-3.6	5.9
KD-05	Coarse Calcite	III	5	85	239.5	-3.6	5.9
KD-05	Coarse Calcite	III	15	90	257.5	-3	5.0
KD-05	Coarse Calcite	III	5	95	214.5	-1.9	3.2
KD-05	Coarse Calcite	III	20	90	269.5	-1.5	2.6
KD-05	Coarse Quartz	III	9	90	250.5		
KD-05	Coarse Quartz	III	6	95	240.5		
KD-05	Coarse Quartz	III	5	95	275.5	-1.9	3.2
KD-05	Coarse Quartz	III	8	90	253.5	-3	5.0
KD-05	Coarse Quartz	III	10	95	263.5	-2.3	3.9
KD-05	Coarse Quartz	III	6	90	246.5	-2.3	3.9
KD-08	Coarse Calcite	III	6	85	244.5	-7.6	11.2
KD-08	Coarse Calcite	III	4	90	191.5	-0.7	1.2
KD-08	Coarse Calcite	III	5	95	211.5	-1.6	2.7
KD-08	Coarse Calcite	III	4	95	263.5	-1.3	2.2
KD-08	Coarse Calcite	III	6	90	243.5	-2	3.4
KD-08	Coarse Calcite	III	8	85	272.5	-0.7	1.2
KD-08	Coarse Calcite	III	6	90	264.5	-0.6	1.1
KD-08	Coarse Calcite	III	10	90	252.5	-1	1.7
KD-08	Coarse Calcite	III	15	90	182.5		
KD-08	Coarse Calcite	III	12	90	268.5	-1	1.7
KD-08	Coarse Calcite	III	8	90	273.5	-1.3	2.2
KD-08	Coarse Qtz	III	10	90	230.5	0.1	0.2
KD-08	Coarse Qtz	III	8	90	186.5	0	0.0
KD-08	Coarse Qtz	III	6	80	256.5	-0.3	0.5
KD-08	Coarse Qtz	III	7	90	229.5	-0.9	1.6
KD-08	Coarse Qtz	III	10	90	212.5	-0.2	0.4
KD-08	Coarse Qtz	III	5	90	224.5	-0.4	0.7
KD-08	Coarse Qtz	III	8	90	294.5	-1.6	2.7
KD-08	Coarse Qtz	III	10	90	278.5	-1.5	2.6
KD-08	Coarse Qtz	III	12	90	288.5	-1.4	2.4
ME-02	Coarse Caclite, Bd. C	III	6	95	270.5	-0.7	1.2
ME-02	Coarse Caclite, Bd. C	III	6	90	287.5	-0.9	1.6

ME-02	Coarse Caclite, Bd. C	III	10	90	201.5		
ME-02	Coarse Caclite, Bd. C	III	12	90	275.5	-0.7	1.2
ME-02	Coarse Caclite, Bd. C	III	6	85	272.5	-0.7	1.2
ME-02	Coarse Caclite, Bd. C	III	4	85	283.5	-0.6	1.1
ME-02	Coarse Calcite Bd. A	III	12	90	255.5	-0.8	1.4
ME-02	Coarse Calcite Bd. A	III	8	80	267.5	-0.8	1.4
ME-02	Coarse Calcite Bd. A	III	8	95	249.5	-0.9	1.6
ME-02	Coarse Calcite Bd. A	III	12	95	253.5	-0.7	1.2
ME-02	Coarse Calcite, Bd. B	III	8	90	297.5	-0.9	1.6
ME-02	Coarse Calcite, Bd. B	III	8	90	269.5	-0.9	1.6
ME-02	Coarse Calcite, Bd. B	III	6	85	281.5	-1.3	2.2
ME-02	Coarse Calcite, Bd. B	III	8	80	284.5	-1.3	2.2
ME-02	Coarse Calcite, Bd. B	III	9	90	285.5	-1.5	2.6
ME-02	Coarse Qtz, Bd. A	III	6	95	297.5	-0.2	0.4
ME-02	Coarse Qtz, Bd. A	III	6	95	268.5	-0.7	1.2
ME-02	Coarse Qtz, Bd. A	III	8	90	271.5	-1.1	1.9
ME-02	Coarse Qtz, Bd. C	III	10	90	237.5	-1.1	1.9
ME-02	Coarse Qtz, Bd. C	III	12	90	242.5	-1.1	1.9
ME-02	Coarse Qtz, Bd. C	III	10	90	189.5	-0.8	1.4
ME-08	Coarse Qtz Vein	III	8	95	262.5	-6.3	9.6
ME-08	Coarse Qtz Vein	III	10	95	261.5	-6.4	9.7
ME-08	Coarse Qtz Vein	III	8	90	274.5	-6	9.2
ME-08	Min Qtz	III	12	85	284.5	-6	9.2
ME-08	Min Qtz	III	6	90	249.5	-2.8	4.6
ME-08	Min Qtz	III	5	90	248.5	-1.8	3.1
ME-08	Min Qtz	III	5	90	235.5	-2.6	4.3
ME-08	Min Qtz	III	12	85	258.5	-2.6	4.3
ME-08	Min Qtz	III	10	90	243.5	-2.3	3.9
OF-1	Calcite	III	15	85	252.5	-2.1	3.5
OF-1	Calcite	III	4	90	269.5	-1.9	3.2
OF-1	Calcite	III	10	90	282.5	-0.4	0.7
OF-1	Calcite	III	12	85	280.5	-0.3	0.5
OF-1	Calcite	III	8	90	281.5	-0.3	0.5
OF-1	Calcite	III	8	85	258.5	-1.8	3.1

OF-1	Calcite	III	6	90	258.5	-1.9	3.2
OF-1	Coarse Qtz	III	12	95	261.5	-5.5	8.5
OF-1	Coarse Qtz	III	7	90	273.5	-4	6.4
OF-1	Coarse Qtz	III	6	95	294.5	-3.8	6.2
OF-1	Coarse Qtz	III	5	85	278.5	-3.8	6.2
OF-1	Coarse Qtz	III	6	90	211.5	-1.5	2.6
OF-1	Coarse Qtz	III	4	90	272.5	-5.1	8.0
OF-1	Coarse Qtz	III	4	90	281.5	-5.2	8.1
OF-1	Coarse Qtz	III	10	90	237.5	-4	6.4
OF-1	Coarse Qtz	III	8	95	240.5	-4	6.4
OF-1	Coarse Qtz	III	6	95	257.5	-3.6	5.9
OF-1	Coarse Qtz	III	8	95	249.5	-3.7	6.0
OF-1	Coarse Qtz	III	8	90	265.5	-6.4	9.7
OF-1	Coarse Qtz	III	8	90	149.5	-2.2	3.7
OF-1	Coarse Qtz	III	8	65	273.5	-3.2	5.3
QF-2	Coarse Opn Slc Qtz	III	5	90	300.5	-1.3	2.2
QF-2	Coarse Opn Slc Qtz	III	15	85	290.5	-2.1	3.5
QF-2	Coarse Opn Slc Qtz	III	8	90	301.5	-1.9	3.2
QF-2	Coarse Opn Slc Qtz	III	10	85	302.5	-2.1	3.5
QF-2	Coarse Opn Slc Qtz	III	13	90	310.5	-1.6	2.7
QF-2	Coarse Opn Slc Qtz	III	10	95	269.5	-1.7	2.9
QF-2	Coarse Opn Slc Qtz	III	8	90	299.5	-1.7	2.9
QF-2	Min Qtz	III	5	85	278.5	-2	3.4
QF-2	Min Qtz	III	6	80	270.5	-2.1	3.5
QF-2	Min Qtz	III	8	70	289.5	-4.6	7.3
QF-2	Min Qtz	III	6	85	288.5	-1.5	2.6
QF-2	Min Qtz	III	8	95	304.5	-1.3	2.2
QF-2	Min Qtz	III	5	80	309.5	-1.5	2.6
QF-2	Min Qtz	III	8	90	281.5	-1.4	2.4
QF-2	Min Qtz	III	6	85	288.5	-1.9	3.2
QF-5	Coarse Opn Slc Qtz	III	8	90	274.5	-4.2	6.7
QF-5	Coarse Opn Slc Qtz	III	6	85	269.5	-4.1	6.6
QF-5	Coarse Opn Slc Qtz	III	6	90	279.5	-4.2	6.7
QF-5	Coarse Opn Slc Qtz	III	12	90	268.5	-3.7	6.0
QF-5	Coarse Opn Slc Qtz	III	8	90	248.5	-3.5	5.7
QF-5	Coarse Opn Slc Qtz	III	15	80	253.5	-3.7	6.0
QF-5	Coarse Qtz	III	15	90	273.5	-1.8	3.1
QF-5	Coarse Qtz	III	9	80	274.5	-1.8	3.1
QF-5	Coarse Qtz	III	6	90	281.5	-1.9	3.2
QF-5	Coarse Qtz	III	6	85	287.5	-1.3	2.2

QF-5	Coarse Qtz	III	7	90	291.5	-1.3	2.2
QF-5	Coarse Qtz	III	12	80	291.5	-1.8	3.1
WC-1	Coarse Qtz	III	10	90	271.5	-1.4	2.4
WC-1	Coarse Qtz	III	6	95	210.5	-5.5	8.5
WC-1	Coarse Qtz	III	10	90	256.5	-6	9.2
WC-1	Coarse Qtz	III	13	95	249.5	-5.8	8.9
WC-1	Coarse Qtz	III	15	95	246.5	-5.9	9.1
WC-1	Coarse Qtz	III	12	90	249.5	-4.6	7.3
WC-1	Coarse Qtz	III	17	95	221.5	-6.6	10.0
WC-1	Coarse Qtz	III	20	95	251.5	-5.2	8.1
WC-1	Coarse Qtz	III	20	90	248.5	-5.2	8.1
WC-1	Coarse Qtz	III	18	95	250.5	-5.2	8.1
WC-1	Coarse Qtz	III	18	90	258.5	-0.5	0.9
WC-1	Coarse Qtz	III	10	95	271.5	-0.6	1.1
WC-1	Coarse Qtz	III	15	95	269.5	-0.2	0.4
WC-1	Coarse Qtz	III	10	90	265.5	-1.4	2.4
WC-1	Coarse Qtz	III	8	95	260.5	-2.1	3.5
WC-1	Coarse Qtz	III	12	90	267.5	-1.4	2.4
WC-1	Coarse Qtz	III	6	95	205.5	-4.6	7.3
WC-1	Coarse Qtz	III	6	95	265.5	-5.2	8.1
WC-1	Coarse Qtz	III	15	95	241.5	-0.6	1.1
WC-1	Coarse Qtz	III	12	95	243.5	-0.8	1.4
WC-1	Coarse Qtz	III	10	90	237.5	-2.2	3.7
WC-1	Coarse Qtz	III	7	95	239.5	-2.5	4.2
SECONDARY INCLUSIONS							
EE-03	Coarse Opn Slc Qtz	Sec.	18	95	194.5	0	0.0
EE-03	Coarse Opn Slc Qtz	Sec.	25	90	227.5	0	0.0
EE-03	Coarse Opn Slc Qtz	Sec.	15	95	168.5	0	0.0
EE-03	Coarse Opn Slc Qtz	Sec.	12	95	186.5	-0.1	0.2
QF-5	Coarse Qtz	Sec.	15	90	167.5	0.1	0.2
QF-5	Coarse Qtz	Sec.	8	95	165.5	0	0.0
QF-5	Coarse Qtz	Sec.	15	95	176.5	0	0.0
QF-5	Coarse Qtz	Sec.	18	90	167.5	-0.3	0.5
QF-5	Coarse Qtz	Sec.	12	95	173.5	-0.3	0.5
QF-5	Coarse Qtz	Sec.	15	95	159.5	-0.4	0.7
QF-5	Coarse Qtz	Sec.	10	90	175.5	-0.3	0.5